Journal of Asian Earth Sciences 124 (2016) 139–155

Contents lists available at ScienceDirect

Journal of Asian Earth Sciences

journal homepage: www.elsevier.com/locate/jseaes

Full length article

A new model for the granite–pegmatite genetic relationships in the Kaluan–Azubai–Qiongkuer pegmatite-related ore fields, the Chinese Altay

Xin Zhang [a,b,c], Hui Zhang [a,*], Zhan-Long Ma [d], Yong Tang [a], Zheng-Hang Lv [a], Jing-Yu Zhao [a,c], Yun-Long Liu [a,c]

[a] Key Laboratory of High-temperature and High-pressure Study of the Earth's Interior, Institute of Geochemistry, Chinese Academy of Sciences, 550002, PR China
[b] School of Earth Sciences and Gansu Key Laboratory of Mineral Resources in Western China, Lanzhou University, Lanzhou 730000, PR China
[c] University of Chinese Academy of Sciences, Beijing 100049, PR China
[d] Exploration Institute of Geology and Mineral Resources of Ningxia, Ningxia 750021, PR China

ARTICLE INFO

Article history:
Received 18 January 2016
Received in revised form 21 April 2016
Accepted 22 April 2016
Available online 30 April 2016

Keywords:
Zircon U–Pb dating
Hf isotopes
Petrogenetic model
Tectonic setting
Chinese Altay

ABSTRACT

Pegmatites commonly form in the waning stage of magma evolution by fractional crystallization of volatile-rich magmas and may be important host rocks of strategic metals (e.g., Li, Be, Cs, Ta, and Nb) and high-quality gem minerals. This study reports new zircon U–Pb dating results and Hf isotopic compositions of the KLA803 pegmatite, the AZB-01 pegmatite, the JMK-09 pegmatite (abbreviated as the K–A–J pegmatites) and the Halong granite from the Chinese Altay to determine the potential petrogenetic relationships between them. The geochronological data document that the K–A–J pegmatites were emplaced at 224.6 ± 2.3 Ma, 191.6 ± 2.0 Ma and 192.0 ± 2.3 Ma, respectively, and they are characterized by negative to low positive $\varepsilon Hf(t)$ values (from −1.0 to +6.3) and old model ages (T_{DM}) (with the T_{DM1} from 874 to 597 Ma and T_{DM2} from 1298 to 833 Ma). In contrast, the Halong granite has an emplacement age of 398.3 ± 2.4 Ma and is characterized by higher positive $\varepsilon Hf(t)$ values (from +9.9 to +15.2) and younger model ages (T_{DM}) (with the T_{DM1} from 626 to 414 Ma and T_{DM2} from 760 to 423 Ma). They all have intruded into the Kulumuti group stratum, which has negative initial $\varepsilon Nd(t)$ values (from −4.3 to −0.2) and old T_{DM} model ages (between 1.22 and 1.56 Ga). Based on the calculated results of the mixing ratios (f) of the initial magmas and the prevailing Paleozoic tectonic framework of the Chinese Altay, we establish two petrogenetic models for the K–A–J pegmatites: Model 1 refers to that these pegmatites originated from a mixed magma that was composed of 72–91 wt.% depleted mantle components and 9–28 wt.% lower crust components; and Model 2 refers to that they were derived from the partial melting of 38–83 wt.% Halong granite and 17–62 wt.% sedimentary rocks from the Kulumuti group. We also suggest that the initial magma of the Halong granite was significantly contributed by juvenile materials with a slight involvement of crustal materials. In Model 1, because LCT-type pegmatites (classified as Li–Cs–Ta enriched pegmatites associated with S-type granite that was produced by the partial melting of preexisting sedimentary rocks) have close geochemical affinities with crustal materials, the excessively high weight percentages (72–91 wt.%) of the depleted mantle components in the initial magma of the K–A–J pegmatites indicate that this model is unrealistic. Therefore, we consider that Model 2 is more reasonable at present for interpreting the petrogenesis of the K–A–J pegmatites, and it needs to be verified in other pegmatite fields of the Chinese Altay.

1. Introduction

Pegmatites are unique rocks, primarily granitic in composition, that are usually characterized by extremely coarse but variable grain size and an abundance of crystals with skeletal, graphic or other strongly directional growth habits (London, 2008). It is widely assumed that pegmatites are formed by magmatic fractional-crystallization and are genetically linked with fertile granitic sources at depth (Jahns and Burnham, 1969; Norton, 1983; London, 1990; Jolliff et al., 1992; Webster et al., 1997; Fuertes-Fuente et al., 2000; Selway and Breaks, 2006; Hulsbosch

* Corresponding author.
E-mail address: zhanghui@vip.gyig.ac.cn (H. Zhang).

http://dx.doi.org/10.1016/j.jseaes.2016.04.020
1367-9120/

et al., 2014). To recognize the granite–pegmatite genetic relationships and evaluate the degree of fractionation, a growing number of studies investigate the geochemical and textural features of the different mineral phases of pegmatites (Baijot et al., 2012; Roda-Robles et al., 2012; Vieira et al., 2011; Lira et al., 2012; Neiva et al., 2008, 2012; Shearer et al., 1992). However, because it is difficult to truly characterize the representative whole-rock geochemical and isotopic features of these coarse-grained rocks, the genetic relationship between pegmatites and host granites is usually not simple to address (Goad and Černý, 1981; Stilling et al., 2006; Černý et al., 2012; Lima et al., 2014).

Zircon is a widely used mineral for isotopic and geochemical studies because of the high contents of trace elements in its crystalline structure and the strong resistance to erosion, weathering and alteration processes. Owing to the close chemical affinities between Hf and Zr, Hf could replace the latter in the zircon crystal lattice with concentrations between 0.3 and 3.3 wt.% (Hoskin and Schaltegger, 2003; Yin et al., 2013). This behavior makes Hf more compatible in zircon than the REEs, especially Lu, leading to low Lu/Hf ratios (typically <0.001). Accordingly, the radioactive decay of ^{176}Lu does not significantly change the Hf isotope composition of zircon with time. Moreover, the low intra-crystalline diffusion rate of Hf in zircon and the high closure temperature of the Lu–Hf isotope system (Cherniak and Watson, 2003) suggest that the effect of post-crystallization thermal events on the Hf isotope composition was small. Hence, the εHf values and T_{DM} model ages of the zircons from pegmatites may provide reliable and significant information on the magma source and the potential genetic relationship with the parental granites (Vervoort et al., 1996; Amelin et al., 2000; Scherer et al., 2000; Griffin et al., 2002; Kinny and Maas, 2003; Hawkesworth and Kemp, 2006; Wang et al., 2008; Lv et al., 2012).

The Central Asian Orogenic Belt is situated among the Siberia, East European, Tarim and North China Cratons, and it represents the largest Phanerozoic accretionary orogenic belt in the world (Fig. 1; Sengör et al., 1993; Sengör and Natalin, 1996; Jahn et al., 2000; Badarch et al., 2002; Chen and Jahn, 2004; Yakubchuk, 2004; Yuan et al., 2007; Xiao et al., 2008, 2009, 2010; Zhou et al., 2008; Biske and Seltmann, 2010; Zhang and Zhang, 2014). As the key part of the CAOB, the Altay orogenic belt lies in Russia, northeastern Kazakhstan, northwestern China and southwestern Mongolia (Fig. 1; Chen and Jahn, 2002). More than 100,000 granitic pegmatite veins are exposed in the Chinese Altay (the Chinese part of the Altay orogenic belt), and many of these pegmatites host economic rare metals such as lithium, beryllium, niobium and tantalum (Wu and Zou, 1989; Wang et al., 2002, 2004). Following earlier work, the geochemistry and mineralogy of the Koktokay No. 3 pegmatite and the Kelumute No. 112 pegmatite continue to be extensively studied (Wang et al., 2002, 2003; Zhu et al., 2006; Lv et al., 2012). More recently, an increasing number of Permian to Jurassic pegmatites have been reported, and the origin of these pegmatites is suggested to be closely related to the late Paleozoic to early Mesozoic post-collision tectonic setting of the Chinese Altay (Fig. 1; Wang et al., 2007; Chen, 2011; Ren et al., 2011; Lv et al., 2012; Ma, 2014). However, the petrogenesis of these pegmatites and the granite–pegmatite genetic relationships still remain uncertain.

The Kaluan ore field, the Azubai ore field and the Qiongkuer ore field (abbreviated as the Kaluan–Azubai–Qiongkuer ore fields or the KAQ ore fields), surrounding and to the west of the Halong granite, contain the pegmatite-type rare-metal deposits of the Kaluan No. 806 and 807 Li deposit, the Kukalagai No. 650 Li deposit and the Qiongkuer No. 1 Nb–Ta deposit (Wu and Zou, 1989; Ma, 2014). Within the KAQ ore fields, the Kaluan No. 803 (KLA803) pegmatite, the Azubai-01 (AZB-01) pegmatite and the Jiamukai-09 (JMK-09) pegmatite (the K–A–J pegmatites) (Fig. 2) are typical of LCT-type pegmatites (classified as Li–Cs–Ta enriched pegmatites associated with S-type granite that was produced by the partial melting of preexisting sedimentary rocks; Černý, 1991; Shelley, 1993; London, 2008), and they are characterized by intensive Be and Ta mineralizations. Geographically, the Halong granite is located approximately 500 m east of the KAQ ore fields and is considered to be the largest granitic batholith in the region (Wu and Zou, 1989; Ma, 2014). Because of the close spatial relationship with the pegmatites in the KAQ ore fields, the Halong granite was assumed to be the parental granite of the pegmatites (Wu and Zou, 1989). Apparently, the identification of the petrogenetic relationship between the K–A–J pegmatites and the Halong granite plays an important role in characterizing the magmatic processes and may greatly benefit further rare metal exploration in the KAQ ore fields. In this study, we perform the geochronological and Hf isotopic studies of the Halong granite and the K–A–J pegmatites to reveal the magmatic sources and the petrogenesis of these formations. Based on the calculated results of the components of the initial magmas, we propose a new petrogenetic model for the K–A–J pegmatites.

2. Geological background

2.1. Regional geology

The Chinese Altay is located in the northern part of Xinjiang Province, extending eastward to Mongolia and westward to Kazakhstan and Russia (Fig. 1, Windley et al., 2002, 2007; Xiao et al., 2004; Long et al., 2007, 2008, 2010; Sun et al., 2008, 2009). On the basis of the stratigraphy, metamorphism, deformation pattern, magmatic activity and geochronology, the Chinese Altay can be divided into five fault-bounded terranes separated by the Hongshanzui, Kalaxianger, Abagong-Kurit and Maerkakuli Faults (Fig. 1; Sengör et al., 1993; Long et al., 2007; Yuan et al., 2007; Sun et al., 2008; Cai et al., 2011a,b). Terrane 1 is made up of Late Devonian to Early Carboniferous clastic sediments, limestones and some minor island-arc volcanic rocks metamorphosed at lower greenschist facies. Terrane 2 is composed of a Middle Ordovician turbidite sequence of lower greenschist facies. Terrane 3 is the largest terrane and is comprised of early Paleozoic sediments metamorphosed at a medium to high grade. Terrane 4 consists of Devonian turbiditic sandstones, pillow basalts and some siliceous volcanic rocks. Terrane 5 is mainly composed of Devonian fossiliferous successions that are, in turn, overlain by Late Carboniferous formations.

The lowermost sedimentary sequence in the Chinese Altay is the Habahe Group, which mostly consists of Ordovician to Sinian thick marine-facies terrigenous clastic rocks including sandstones, siltstones and mudstones (BGMRX, 1993; Windley et al., 2002; Long et al., 2007). The recent U–Pb dating of the detrital zircons and the whole-rock geochemical studies of the sedimentary rocks of the Habahe Group suggest that these strata were deposited along an active continental margin predominately during the Silurian (Long et al., 2007, 2008, 2010). Additionally, the marine-facies metasediments of the Kulumuti Group ($S_{2\text{-}3}$KL) unconformably overlie the Habahe sequence in the central part of the Chinese Altay (BGMRX, 1993). All of these strata were intruded by early to middle Paleozoic arc-related plutons and late Paleozoic post-collision A-type granites (Fig. 1; Han et al., 1997; Chen and Jahn, 2002, 2004; Chen and Arakawa, 2005; Su et al., 2006; Wang et al., 2006; Yuan et al., 2007; Zhou et al., 2008; Tang et al., 2010; Cai et al., 2011a,b, 2012; Shen et al., 2011).

Abundant NW-SE trending faults occur in the Chinese Altay, such as the Hongshanzui, Kalaxianger, Abagong-Kurit, Bazhai, Maerkakuli and Erqis Faults (Fig. 1). As one of the largest transcurrent

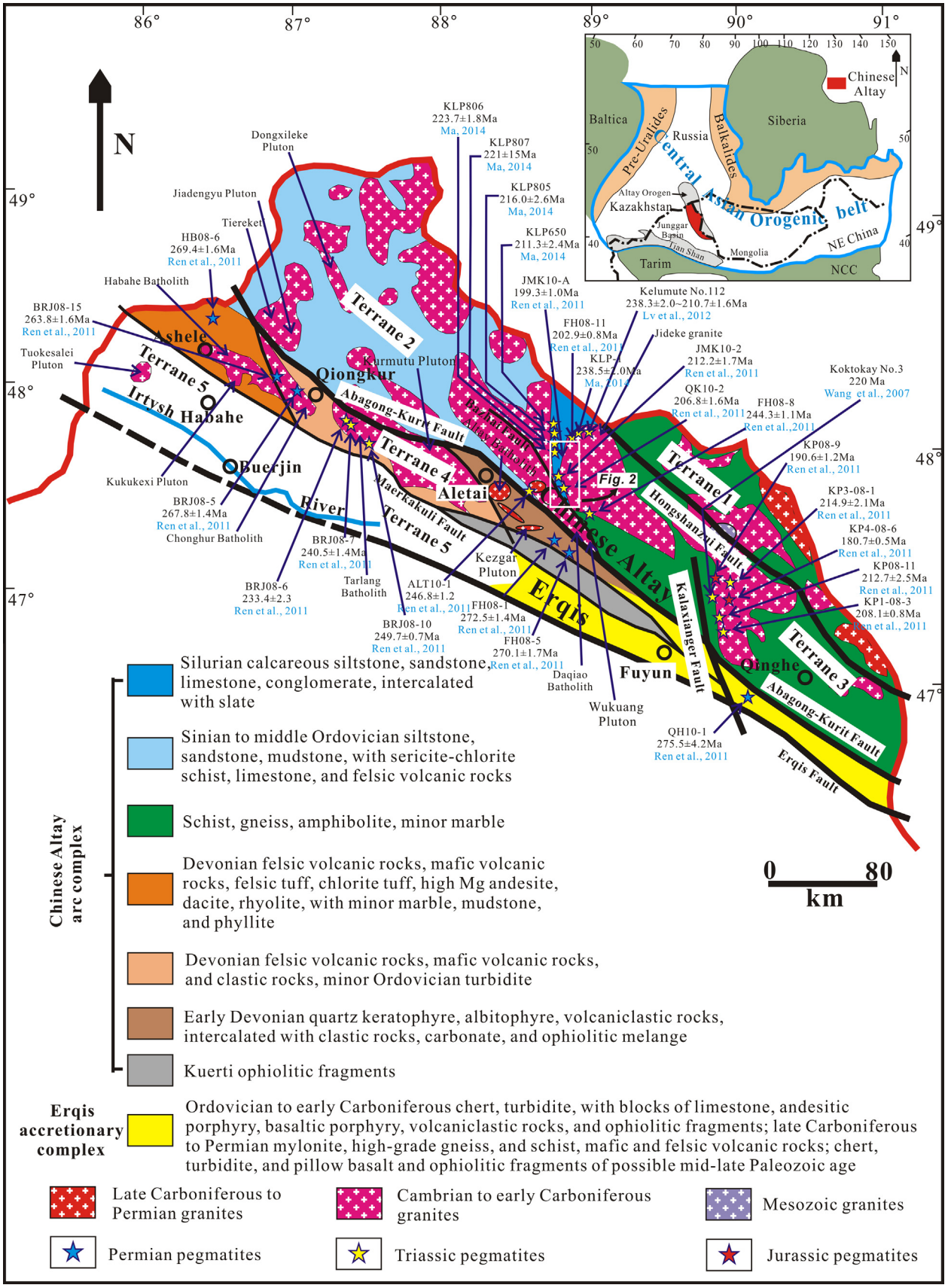

Fig. 1. The geological map of the Chinese Altay (modified after Xiao et al., 2009; Cai et al., 2010; Xiao and Santosh, 2014; the age data are from Wang et al., 2007, 2011; Chen, 2011; Cai et al., 2010; Ren et al., 2011; Shen et al., 2011; Lv et al., 2012; Ma, 2014).

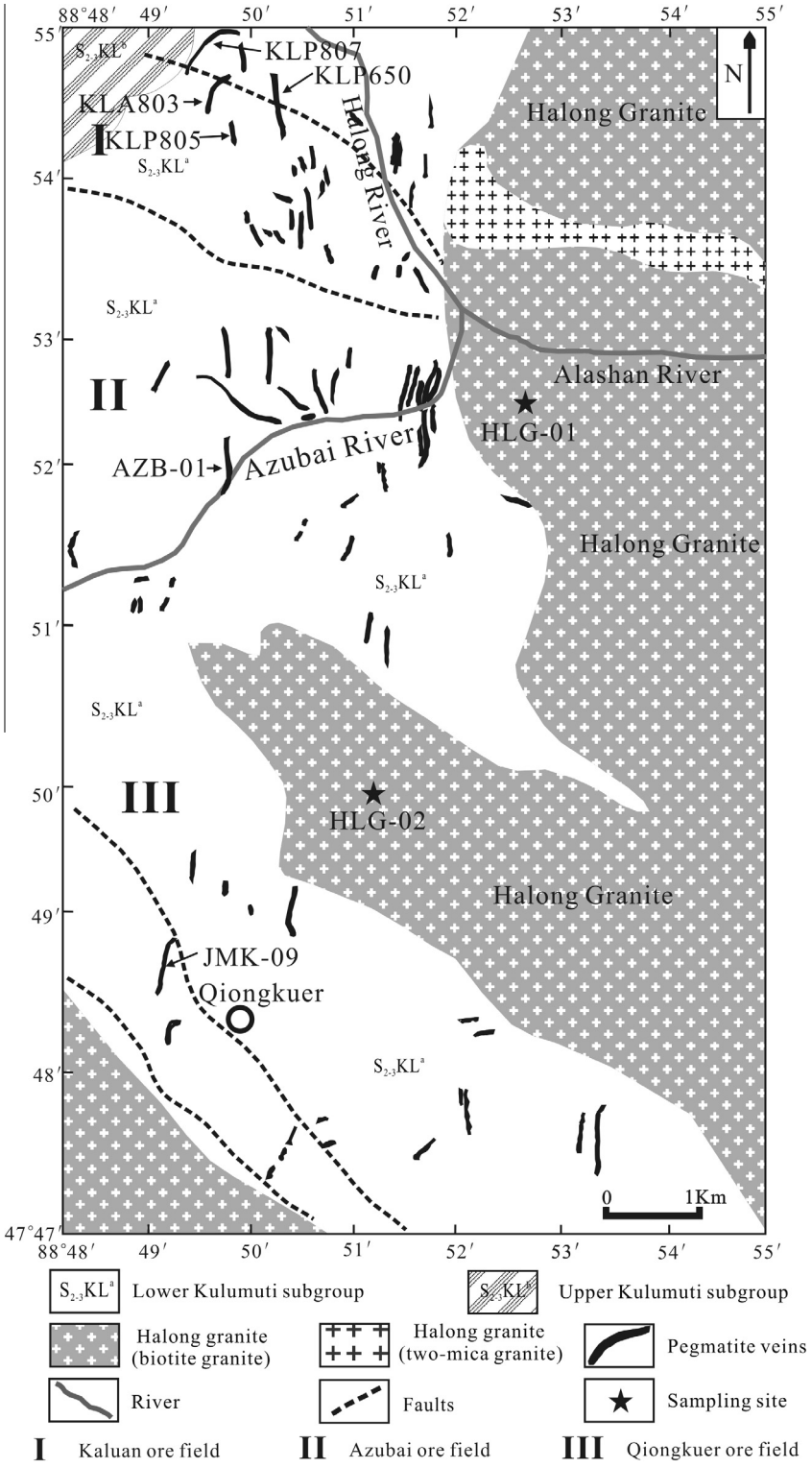

Fig. 2. The geological map of the Kaluan–Azubai–Qiongkuer ore field (modified after Ma, 2014).

faults in central Asia, the Erqis Fault forms the boundary between the Altay orogenic belt and the Kazakhstan block (Sengör et al., 1993; Wang et al., 2006). This fault zone contains an ophiolite with a zircon U–Pb age of 390 Ma, and it is assumed to be the site of an early to middle Paleozoic subduction (Wang et al., 2003). During the late Paleozoic, this fault zone experienced a large-scale sinistral displacement (Laurent-Charvet et al., 2003; Windley et al., 2007; Briggs et al., 2009).

2.2. Geology of the Kaluan–Azubai–Qiongkuer ore fields

The Kaluan–Azubai–Qiongkuer (KAQ) ore fields are situated in the central part of the Chinese Altay in Xinjiang Province and are approximately 75 km northeast from Aletai City (Fig. 2). According to the previous work, more than 10,000 pegmatite veins are exposed in the KAQ ore fields, and a portion of these pegmatites host economic rare-metal deposits (Wu and Zou, 1989; Ma, 2014).

The exposed stratum in the KAQ ore fields mainly consists of the Kulumuti group ($S_{2-3}KL$), which is considered as a Silurian turbiditic sequence comprising siltstone and sandstone that have been pervasively metamorphosed into moderate-grained mica schist (Fig. 2; Windley et al., 2002; Wang et al., 2014). This group has a total thickness of approximately 8000 m and is subdivided into two subgroups based on the differences in lithofacies. The Upper Kulumuti group ($S_{2-3}KL^b$) is grey, light-grey and green in color and mainly includes homogenic migmatite, plagiogneiss, staurolite–schist, andalusite–schist, chlorite–schist, sericite–schist, metasandstone and calcareous sandstone. The Lower Kulumuti group ($S_{2-3}KL^a$) is also grey, light-grey and green in color and involves biotite–cordierite–quartz schist, biotite–gneiss, migmatite, chlorite–schist and muscovite–biotite schist (BGMRX, 1993; Windley et al., 2002; Cai et al., 2011c).

2.3. Field relationship and petrography

The KLA803 pegmatite, a LCT-type pegmatite, intruded in the Late Silurian sedimentary rocks (the Lower Kulumuti group, $S_{2-3}KL^a$) with a length of approximately 480 m and a width of 2 m. The textural zonation of this pegmatite is not obvious, and only the graphic pegmatite zone and the quartz–albite–spodu mene zone can be distinguished at the outcrop. The exposed rocks mainly belong to the quartz–albite–spodumene zone, including the rock-forming minerals of quartz, albite, spodumene, microcline and muscovite (Fig. 3a).

The AZB-01 pegmatite is a Be-mineralized pegmatite. A substantial amount of beryl crystals are hosted in the graphic pegmatite zone. This pegmatite vein shows a NS-trend with a dip angle of 40°, and it is approximately 450 m in length and 3 m in width. The exposed rocks primarily consist of quartz, albite, muscovite and microcline (Fig. 3b).

The JMK-09 pegmatite is a Nb and Ta-mineralized pegmatite hosting considerable volumes of columbite–tantalite. This pegmatite is located to the northwest of Qiongkuer Village and shows a NE-trend. The pegmatite vein is approximately 480 m in length and is 2–3 m in width with a dip angle of 50°. The textural zonation of this pegmatite is difficult to distinguish, and the exposed rocks are complicated. The rock-forming minerals are mainly quartz, albite, muscovite, microcline and columbite–tantalite (Fig. 3c).

The Halong granite is situated in the southeastern part of Terrane 2 of the Chinese Altay, and it is considered to be a granitic batholith covering an area of approximately 600 km^2. In the hand specimen, the rock samples are light-grey in color with a massive structure and a granitic texture (Fig. 3d). The rock-forming minerals mainly include quartz (25–30%), plagioclase (35–40%), potash feldspar (25–33%), biotite (6–10%) and muscovite (2–4%) (Fig. 3d–f).

3. Samples and analytical methods

The evolution of pegmatitic magmas includes magmatic, magmatic–hydrothermal transition and hydrothermal stages, which correspond to the internal zonations (from border to core) of pegmatitic veins (Burnham and Ohmoto, 1980; London, 1986, 2005; Morgan and London, 1999). Because the crystallization of the zircons from the border zone of a pegmatite is dominantly controlled by magmatic stage and has not been affected by the magmatic hydrotherm, the U–Pb age of these zircons could represent the emplacement age of the pegmatite (Lv et al., 2012). To avoid the late-stage hydrothermal effects, the pegmatite samples were selected from the border zones, and all of the samples were fresh and of sufficient mass (>10 kg) to satisfy the requirements for zircon quality and quantity. To constrain the emplacement age correctly, we collected two samples (HLG-01 and HLG-02) without lithological differences as fresh as possible for the zircon U–Pb dating. The specific sampling sites of the pegmatites and the Halong granite are shown in Fig. 2.

The zircon grains from the KLA803 pegmatite, AZB-01 pegmatite, JMK-09 pegmatite and the Halong granite were concentrated by using heavy-liquid and magnetic methods, and the individual zircon grains were finally handpicked under a binocular microscope. The zircon target preparation, image acquisition under reflected light and cathodoluminescence (CL), and in situ U–Pb analyses using laser ablation inductively coupled plasma mass spectrometry (LA-ICPMS) were performed at Hefei University of Technology, Hefei. The sample mounts were placed in a two-volume sample cell flushed with Ar and He. The laser ablation was operated at a constant energy of 80 mJ and at 8 Hz with a spot diameter of 31 μm. The ablated material was carried by He gas to the Aglient 7500a ICP-MS for U–Pb isotopic analysis. The corrections were included for the mass bias drift, which was referenced using the standard of the NIST 610 glass (Pearce et al., 1997). The Temora was used as the age standard ($^{206}Pb/^{238}U$ = 416.8 Ma) (Black et al., 2003). The trace-element concentrations of U, Th and Pb were determined by normalizing the count rates for each analyzed element to those for Si and assuming SiO_2 as stoichiometric in zircon. The apparent and concordant U–Pb ages were calculated using the ISOPLOT program (Ludwig, 2003).

The zircon Hf in situ isotopic analysis was conducted by employing a 193 nm ArF excimer laser ablation system attached to a Neptune Plasma Multicollector-ICP-MS at the State Key Laboratory of Continental Dynamics, Department of Geology, Northwest University, Xi'an. The analysis was undertaken under a laser repetition rate of 10 Hz at 200 mJ and an ablated spot size of 60 μm. The detailed analytical procedures were described by Xu et al. (2004) and Wu et al. (2006). The $^{176}Hf/^{177}Hf$ ratio of 0.282307 ± 24 (2σ, N = 11), obtained by our analysis, varied in accordance with 0.282302 ± 8 (2σ), as determined using the solution method for the zircon standard 91500 (Goolaerts et al., 2004; Woodhead et al., 2004).

4. Results

4.1. Zircon U–Pb geochronology

4.1.1. KLA803 pegmatite

The zircon grains of the KLA803 pegmatite vary from 100 to 200 μm in size and from brown to dark brown in color with opaque, euhedral tetragonal-dipyramid or stubby tetragonal prism shapes (Fig. 4a). The grains show taxitic and mottled textures with a weak cathodoluminescence (CL). These features can be explained by the radiation damage of U^{4+}, which may suppress the CL emission of zircon (Rubatto and Gebauer, 2000; Corfu et al., 2003; Hanchar and Hoskin, 2003). The Th and U contents of the analytical spots ranged from 40 to 5991 ppm and from 1913 to 70,047 ppm, with Th/U ratios ranging from 0.02 to 0.50.

A total of nineteen zircons from the KLA803 pegmatite were selected to determine the U and Pb isotopic compositions (Table 1). Six of the nineteen spots that yield older $^{206}Pb/^{238}U$ ages from 373 Ma to 265 Ma evidently deviate from the concordant line in the diagram (Fig. 5a), and they are most likely to be xenocrysts because of the relatively high Th/U ratios (from 0.10 to 0.50, Table 1). One spot (KLA803-02) yielded a meaningless younger $^{206}Pb/^{238}U$ age of 200 Ma, possibly because of the radioactive Pb loss (Lv et al., 2012). The other twelve spots define an extraordinarily similar age population (from 227 to 223 Ma) and yielded a weighted mean $^{206}Pb/^{238}U$ age of 224.6 ± 2.3 Ma (Fig. 5a), which most likely represents the crystallization age of the zircons of the KLA803 pegmatite.

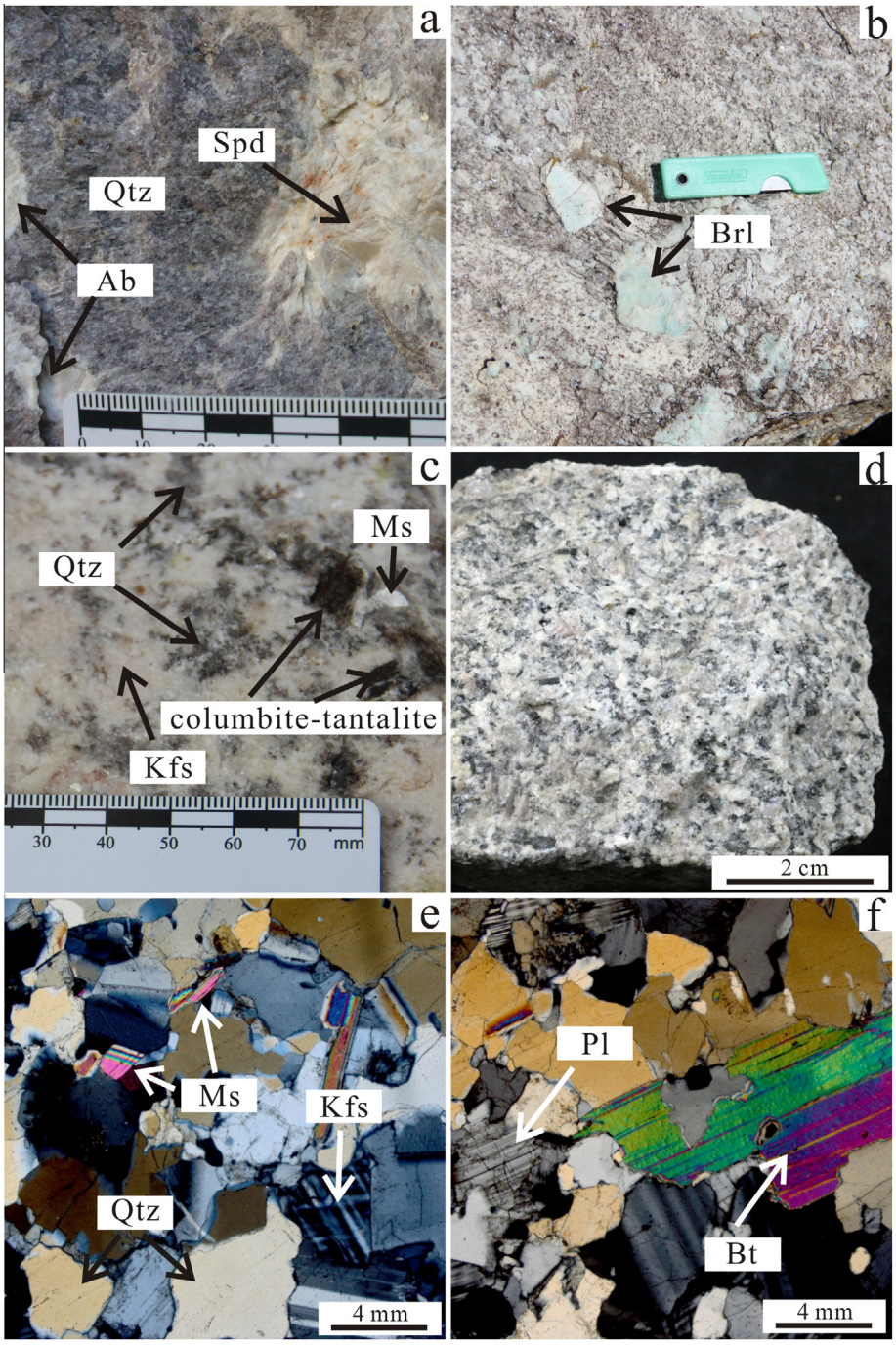

Fig. 3. The photographs and micrographs of the KLA803 pegmatite, the AZB-01 pegmatite, the JMK-09 pegmatite and the Halong granite: (a) the photograph of the KLA803 pegmatite showing the spodumene crystals; (b) the photograph of the AZB-01 pegmatite showing the crystals of beryl; (c) the photograph of the JMK-09 pegmatite showing the dark minerals of columbite–tantalite; (d) the photograph of the Halong granite in the hand specimen; (e) the micrograph of the Halong granite, including rock-forming minerals of muscovite, quartz and K-feldspar; (f) the micrograph of the Halong granite with plagioclase and large size muscovite. Ab: albite, Ms: muscovite, Qtz: quartz, Kfs: K-feldspar, Brl: beryl, Pl: plagioclase, Bt: Biotite; Spd: spodumene.

4.1.2. AZB-01 pegmatite

The zircon grains of the AZB-01 pegmatite vary from 100 to 250 μm in size with a euhedral tetragonal-dipyramid or stubby tetragonal prism shape (Fig. 4b). The mantles and cores of these zircons usually show taxitic and mottled textures with a weak cathodoluminescence (CL). The zircons of the spots of AZB-01-06 and AZB-01-10 exhibit a porous and spongy texture, which may result from the high U contents (i.e., 11,620 ppm and 13,939 ppm). The Th and U contents of the analytical spots ranged from 13 to 406 ppm and from 1008 to 13,939 ppm, with Th/U ratios ranging from 0.01 to 0.06 (Table 1).

Nineteen zircons from the AZB-01 pegmatite were selected for the determinations of the U and Pb isotopic compositions. The $^{206}Pb/^{238}U$ ages of these zircons vary from 205.9 to 186.5 Ma, in which, sixteen spots yielded concordant ages from 196.9 to 186.5 Ma and a weighted mean age of 191.6 ± 2.0 Ma. Three other spots that exhibited weak CL yielded meaningless ages of 205.9, 205.8 and 205.0 Ma, possibly because of the high contents of U

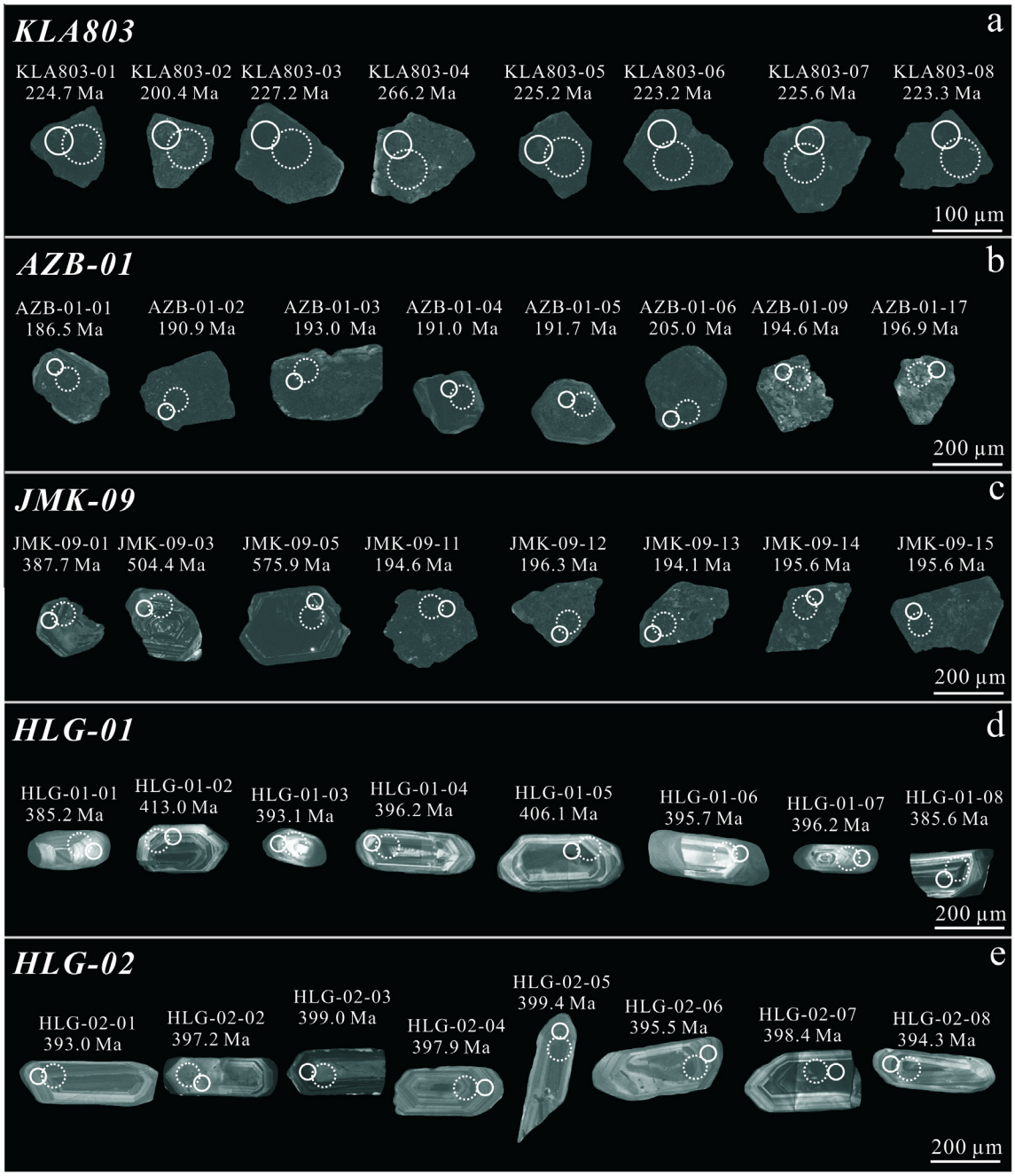

Fig. 4. The CL images of zircons from the KLA803 pegmatite, AZB-01 pegmatite, JMK-09 pegmatite and the Halong granite (HLG-01 and HLG-02).

(6102–13,939 ppm). Therefore, the weighted mean age of 191.6 ± 2.0 Ma probably represents the formation age of the AZB-01 pegmatite (Fig. 5b).

4.1.3. JMK-09 pegmatite

The zircon grains of the JMK-09 pegmatite vary from 100 to 250 μm in size and are dark brown in color with a subhedral tetragonaldipyramid or euhedral stubby tetragonal prism shape (Fig. 4c). A number of zircons (i.e., the spots of JMK-09-01, JMK-09-03 and JMK-09-05) exhibit blurred remnants of the original oscillatory zoning. The Th and U contents of the analytical spots ranged from 2 to 928 ppm and from 1531 to 8656 ppm, with Th/U ratios ranging from 0.002 to 0.14.

A total of seventeen zircons were selected to determine the U–Pb isotopic compositions, yielding $^{206}Pb/^{238}U$ ages from 577.6 to 193.0 Ma (Table 1). Ten of the seventeen spots that exhibit blurred remnants of the original zoning, as shown in the CL images, yield much older ages from 577.6 to 350.3 Ma, indicating that these zircons are likely xenocrysts (i.e., the spots of JMK-09-01, JMK-09-03 and JMK-09-05). The other seven spots are close to the concordant line and yield a weighted mean age of 192.0 ± 2.3 Ma (Fig. 5c). We consider this age to be the zircon crystallization time.

4.1.4. HLG-01

The zircon grains from sample HLG-01 are 100–300 μm in size and pale yellow in color with a euhedral spindly or stubby tetragonal prism shape. All of the zircons show a bright CL and clear concentric oscillatory zones (Fig. 4d). The Th and U contents of the analytical spots ranged from 67 to 1136 ppm and from 108 to 3314 ppm, respectively, with the Th/U ratios ranging from 0.12

Table 1
The zircon U–Pb dating results of the KLA803 pegmatite, the AZB-01 pegmatite, the JMK-09 pegmatite and the Halong granite (HLG-01 and HLG-02), determined by LA-ICP-MS.

Sample	Th (ppm)	U (ppm)	Th/U	Ratio						Age (Ma)			
				$^{207}Pb/^{206}Pb$	1σ	$^{207}Pb/^{235}U$	1σ	$^{206}Pb/^{238}U$	1σ	$^{207}Pb/^{235}U$	1σ	$^{206}Pb/^{238}U$	1σ
KLA803													
KLA803-01	291	3295	0.088	0.09209	0.00321	0.46102	0.02149	0.03548	0.00061	385.0	15	224.7	4
KLA803-02	2395	70047	0.034	0.17674	0.00754	0.78421	0.04641	0.03158	0.00069	587.9	26	200.4	4
KLA803-03	186	5143	0.036	0.11312	0.00316	0.55952	0.01796	0.03587	0.00057	451.2	12	227.2	4
KLA803-04	364	3576	0.102	0.30695	0.01228	1.81830	0.09473	0.04217	0.00079	1052.1	34	266.2	5
KLA803-05	129	3185	0.041	0.10682	0.00452	0.52839	0.02633	0.03555	0.00059	430.7	17	225.2	4
KLA803-06	67	2026	0.033	0.08467	0.00376	0.41037	0.01942	0.03522	0.00066	349.1	14	223.2	4
KLA803-07	343	5379	0.064	0.10114	0.00339	0.49901	0.01842	0.03561	0.00038	411.0	12	225.6	2
KLA803-08	270	8160	0.033	0.17969	0.00508	0.87751	0.02757	0.03524	0.00044	639.6	15	223.3	3
KLA803-09	1327	5789	0.229	0.13199	0.00372	0.77583	0.02406	0.04235	0.00059	583.1	14	267.4	4
KLA803-10	169	2091	0.081	0.07783	0.00231	0.38097	0.01174	0.03524	0.00050	327.8	9	223.3	3
KLA803-11	188	4831	0.039	0.07759	0.00214	0.38133	0.01142	0.03530	0.00047	328.0	8	223.6	3
KLA803-12	40	1913	0.021	0.14267	0.00829	0.74091	0.05263	0.03573	0.00075	562.9	31	226.3	5
KLA803-13	5991	18,857	0.318	0.27727	0.00620	1.62048	0.04693	0.04201	0.00071	978.2	18	265.3	4
KLA803-14	250	2566	0.097	0.14337	0.00414	0.84586	0.03034	0.04230	0.00064	622.4	17	267.0	4
KLA803-15	370	4005	0.092	0.09814	0.00305	0.46732	0.02052	0.03590	0.00235	389.3	14	227.3	15
KLA803-16	1271	3679	0.346	0.19280	0.00588	1.60955	0.07020	0.05951	0.00130	973.9	27	372.7	8
KLA803-17	4643	9321	0.498	0.25645	0.00624	2.11096	0.07902	0.05970	0.00191	1152.4	26	373.8	12
KLA803-18	298	7701	0.039	0.17572	0.00696	0.87575	0.05054	0.03523	0.00056	638.7	27	223.2	4
KLA803-19	148	5185	0.029	0.17967	0.00467	0.89653	0.03342	0.03562	0.00059	649.9	18	225.6	4
AZB-01													
AZB-01-01	13	1008	0.013	0.04871	0.00333	0.19707	0.01343	0.02935	0.00027	182.6	11	186.5	2
AZB-01-02	101	6637	0.015	0.06587	0.00583	0.27628	0.02489	0.03006	0.00032	247.7	20	190.9	2
AZB-01-03	406	6363	0.064	0.07084	0.00203	0.29776	0.00816	0.03039	0.00027	264.7	6	193.0	2
AZB-01-04	100	3345	0.030	0.07649	0.01071	0.32657	0.04625	0.03008	0.00033	286.9	35	191.0	2
AZB-01-05	36	1459	0.025	0.10931	0.01777	0.45292	0.07342	0.03019	0.00052	379.3	51	191.7	3
AZB-01-06	160	11620	0.014	0.12244	0.01971	0.54780	0.08776	0.03231	0.00030	443.6	58	205.0	2
AZB-01-07	76	7920	0.010	0.06322	0.01096	0.33269	0.07651	0.03026	0.00074	291.6	58	192.2	5
AZB-01-08	22	2308	0.010	0.05393	0.00658	0.22373	0.02722	0.03005	0.00029	205.0	23	190.9	2
AZB-01-09	62	2593	0.024	0.05735	0.00456	0.24336	0.01920	0.03064	0.00029	221.2	16	194.6	2
AZB-01-10	151	13939	0.011	0.10045	0.00530	0.45593	0.02516	0.03245	0.00037	381.4	18	205.9	2
AZB-01-11	118	6102	0.019	0.09907	0.00251	0.44158	0.01059	0.03244	0.00039	371.4	7	205.8	2
AZB-01-12	52	1517	0.034	0.14999	0.00664	0.66419	0.04012	0.03016	0.00055	517.2	24	191.6	3
AZB-01-13	91	1515	0.060	0.07419	0.00908	0.34504	0.05862	0.02937	0.00060	301.0	44	186.6	4
AZB-01-14	119	3673	0.032	0.10011	0.00207	0.42202	0.00980	0.03036	0.00034	357.5	7	192.8	2
AZB-01-15	104	3760	0.028	0.11905	0.00309	0.51081	0.01514	0.03079	0.00038	419.0	10	195.5	2
AZB-01-16	94	3311	0.028	0.08644	0.00284	0.36394	0.01411	0.02995	0.00034	315.2	11	190.2	2
AZB-01-17	85	2644	0.032	0.11611	0.00277	0.50358	0.01449	0.03102	0.00035	414.1	10	196.9	2
AZB-01-18	32	2010	0.016	0.07599	0.00174	0.31823	0.00776	0.03015	0.00030	280.5	6	191.5	2
AZB-01-19	64	3423	0.019	0.07334	0.00244	0.30793	0.01158	0.02993	0.00032	272.6	9	190.1	2
JMK-09													
JMK-09-01	38	3675	0.010	0.06637	0.00723	0.64483	0.08008	0.06198	0.00083	505.3	49	387.7	5
JMK-09-02	21	3642	0.006	0.06437	0.00133	0.60688	0.01323	0.06208	0.00060	481.6	8	388.3	4
JMK-09-03	386	5803	0.067	0.11308	0.00710	1.39729	0.09905	0.08139	0.00085	887.8	42	504.4	5
JMK-09-04	52	4062	0.013	0.11072	0.00406	1.32368	0.05558	0.08124	0.00083	856.1	24	503.5	5
JMK-09-05	492	6787	0.072	0.13803	0.00320	1.82686	0.04579	0.09344	0.00114	1055.2	16	575.9	7
JMK-09-06	166	4995	0.033	0.11228	0.00289	1.48534	0.03820	0.09340	0.00103	924.4	16	575.6	6
JMK-09-07	2	1531	0.002	0.06814	0.00219	0.92548	0.03499	0.09289	0.00173	665.3	18	572.6	10
JMK-09-08	691	8656	0.080	0.16378	0.00988	2.31322	0.15379	0.09373	0.00200	1216.3	47	577.6	12
JMK-09-09	206	4849	0.042	0.16201	0.00516	1.36921	0.04770	0.05585	0.00116	875.8	20	350.3	7
JMK-09-10	928	6670	0.139	0.16107	0.01267	1.69860	0.18638	0.06200	0.00152	1008.0	70	387.8	9
JMK-09-11	145	5227	0.028	0.09549	0.00269	0.41168	0.01331	0.03065	0.00052	350.1	10	194.6	3
JMK-09-12	87	8201	0.011	0.06106	0.00181	0.26789	0.00967	0.03092	0.00058	241.0	8	196.3	4
JMK-09-13	155	5324	0.029	0.07533	0.00239	0.32772	0.01191	0.03056	0.00066	287.8	9	194.1	4
JMK-09-14	150	8087	0.019	0.09413	0.00316	0.40981	0.01388	0.03080	0.00076	348.7	10	195.6	5
JMK-09-15	99	3140	0.032	0.07050	0.00216	0.31145	0.01128	0.03081	0.00092	275.3	9	195.6	6
JMK-09-16	74	3877	0.019	0.07560	0.00189	0.32986	0.00830	0.03063	0.00100	289.5	6	194.5	6
JMK-09-17	61	6011	0.010	0.06578	0.00295	0.28880	0.01413	0.03039	0.00111	257.6	11	193.0	7
HLG-01													
HLG-01-01	684	659	1.038	0.05258	0.00331	0.45508	0.02650	0.06158	0.00129	380.8	18	385.2	8
HLG-01-02	1136	330	3.439	0.05163	0.00336	0.47699	0.02964	0.06617	0.00141	396.0	20	413.0	9
HLG-01-03	310	511	0.607	0.05781	0.00408	0.50639	0.03400	0.06288	0.00145	416.0	23	393.1	9
HLG-01-04	340	582	0.585	0.05560	0.00307	0.49417	0.02672	0.06339	0.00124	407.7	18	396.2	8
HLG-01-05	192	1164	0.165	0.05364	0.00145	0.49108	0.01308	0.06503	0.00071	405.6	9	406.1	4
HLG-01-06	506	1924	0.263	0.05311	0.00158	0.47411	0.01343	0.06331	0.00077	394.0	9	395.7	5
HLG-01-07	139	303	0.457	0.05575	0.00258	0.48692	0.02064	0.06339	0.00108	402.8	14	396.2	7
HLG-01-08	143	299	0.480	0.05135	0.00364	0.43842	0.02891	0.06163	0.00163	369.1	20	385.6	10
HLG-01-09	726	3314	0.219	0.05300	0.00139	0.47275	0.01216	0.06316	0.00074	393.1	8	394.8	4
HLG-01-10	267	381	0.703	0.05445	0.00200	0.48490	0.01638	0.06418	0.00092	401.4	11	401.0	6
HLG-01-11	378	183	2.070	0.05467	0.00255	0.48186	0.02242	0.06410	0.00110	399.3	15	400.5	7
HLG-01-12	479	344	1.391	0.05373	0.00196	0.49297	0.01829	0.06500	0.00093	406.9	12	406.0	6

Table 1 (*continued*)

Sample	Th (ppm)	U (ppm)	Th/U	Ratio						Age (Ma)			
				$^{207}Pb/^{206}Pb$	1σ	$^{207}Pb/^{235}U$	1σ	$^{206}Pb/^{238}U$	1σ	$^{207}Pb/^{235}U$	1σ	$^{206}Pb/^{238}U$	1σ
HLG-01-13	473	294	1.607	0.05367	0.00279	0.48778	0.02380	0.06509	0.00119	403.4	16	406.5	7
HLG-01-14	67	337	0.200	0.05439	0.00297	0.49617	0.02438	0.06516	0.00135	409.1	17	406.9	8
HLG-01-15	412	212	1.938	0.05767	0.00307	0.51157	0.02569	0.06399	0.00129	419.5	17	399.8	8
HLG-01-16	222	108	2.052	0.06468	0.00427	0.54131	0.02971	0.06430	0.00180	439.3	20	401.7	11
HLG-01-17	96	785	0.122	0.05231	0.00211	0.47271	0.01864	0.06407	0.00088	393.1	13	400.3	5
HLG-01-18	255	159	1.607	0.06128	0.00335	0.52938	0.02565	0.06374	0.00116	431.4	17	398.3	7
HLG-02													
HLG-02-01	724	828	0.87	0.04901	0.00184	0.43124	0.01465	0.06286	0.00079	364.1	10	393.0	5
HLG-02-02	179	448	0.40	0.04894	0.00182	0.43500	0.01500	0.06356	0.00085	366.7	11	397.2	5
HLG-02-03	150	730	0.20	0.05024	0.00145	0.44847	0.01202	0.06386	0.00067	376.2	8	399.0	4
HLG-02-04	221	591	0.37	0.05304	0.00178	0.47230	0.01511	0.06367	0.00078	392.8	10	397.9	5
HLG-02-05	308	401	0.77	0.05087	0.00195	0.45002	0.01589	0.06392	0.00086	377.3	11	399.4	5
HLG-02-06	140	360	0.39	0.05316	0.00236	0.47461	0.02236	0.06335	0.00095	394.4	15	395.9	6
HLG-02-07	202	335	0.60	0.04945	0.00196	0.43820	0.01693	0.06376	0.00082	369.0	12	398.4	5
HLG-02-08	199	461	0.43	0.05277	0.00206	0.46320	0.01762	0.06307	0.00087	386.5	12	394.3	5
HLG-02-09	365	724	0.50	0.05358	0.00189	0.47741	0.01638	0.06361	0.00076	396.3	11	397.6	5
HLG-02-10	48	150	0.32	0.05224	0.00334	0.44905	0.02692	0.06347	0.00121	376.6	19	396.7	7
HLG-02-11	107	198	0.54	0.05487	0.00241	0.48556	0.01960	0.06430	0.00091	401.9	13	401.7	6
HLG-02-12	171	253	0.67	0.05205	0.00227	0.45146	0.01765	0.06334	0.00100	378.3	12	395.9	6
HLG-02-13	190	321	0.59	0.05107	0.00195	0.45291	0.01608	0.06374	0.00097	379.3	11	398.3	6
HLG-02-14	46	241	0.19	0.05456	0.00246	0.47852	0.01995	0.06361	0.00114	397.1	14	397.5	7
HLG-02-15	197	410	0.48	0.05001	0.00176	0.44159	0.01495	0.06350	0.00079	371.4	11	396.9	5
HLG-02-16	151	363	0.42	0.05617	0.00194	0.50055	0.01748	0.06353	0.00092	412.1	12	397.1	6
HLG-02-17	140	509	0.27	0.04969	0.00229	0.44241	0.01988	0.06340	0.00086	371.9	14	396.3	5
HLG-02-18	121	283	0.43	0.05289	0.00253	0.46789	0.02084	0.06356	0.00109	389.7	14	397.2	7

to 3.44 (Table 1). These characteristics indicate that the zircons of this sample are magmatic in origin.

The U–Pb isotope analytical results for the eighteen zircons of the HLG-01 are listed in Table 1. All of the spots are close to the concordant line in the $^{206}Pb/^{238}U$ vs. $^{207}Pb/^{235}U$ concordia diagram and yield a weighted average age of 399.7 ± 2.9 Ma (Fig. 5d).

4.1.5. HLG-02

The zircon grains from sample HLG-02 are 100–350 μm in size and yellow in color with euhedral tetragonal prism shapes (Fig. 4e). The CL images of the zircons exhibit a clear and periodic zonal texture. The Th and U contents of the analytical spots ranged from 46 to 724 ppm and from 150 to 828 ppm, respectively, with the Th/U ratios ranging from 0.19 to 0.87, indicating that these zircons are also magmatic in origin (Table 1).

Eighteen zircons for the determinations of the U and Pb isotopic compositions were selected from the domains of bright CL, homogenous composition and clear oscillatory zoning. All of the spots yield a similar age population of 410.7 to 393.0 Ma with a weighted mean age of 397.3 ± 2.4 Ma (Fig. 5e).

In combination with the sample of HLG-01, a total of 36 spots yield a weighted mean age of 398.3 ± 2.4 Ma (MSWD = 0.57, Probability = 0.98; Fig. 5f). We consider that this age is the emplacement age of the Halong granite.

4.2. Zircon Hf isotopic compositions

4.2.1. KLA803 pegmatite

Fifteen spots of the zircons of the KLA803 pegmatite exhibit nearly identical $^{176}Hf/^{177}Hf$ values from 0.28263 to 0.28271 (Table 2). According to the crystallization age of 225 Ma, the calculated εHf(t) values ranged from −0.6 to +2.2 with the T_{DM1} model ages ranging from 858 to 748 Ma and T_{DM2} model ages ranging from 1275 to 1095 Ma.

4.2.2. AZB-01 pegmatite

Fifteen zircon grains of the AZB-01 pegmatite yielded $^{176}Hf/^{177}Hf$ values ranging from 0.28262 to 0.28283. Based on the crystallization age of 192 Ma, the calculated εHf(t) values are from −1.0 to +6.3, with the T_{DM1} model ages ranging from 874 to 597 Ma and the T_{DM2} model ages ranging from 1298 to 833 Ma (Table 2).

4.2.3. JMK-09 pegmatite

Fifteen spots of the zircons of the JMK-09 pegmatite exhibit nearly identical $^{176}Hf/^{177}Hf$ values ranging from 0.28266 to 0.28274 (Table 2). According to the crystallization age of 192 Ma, the calculated εHf(t) values ranged from +0.4 to +3.3 with the T_{DM1} model ages ranging from 817 to 708 Ma and the T_{DM2} model ages ranging from 1208 to 1028 Ma.

4.2.4. HLG-01

Eleven spots of sample HLG-01 yielded $^{176}Hf/^{177}Hf$ values ranging from 0.28283 to 0.28296 (Table 2). Based on the crystallization age of 398 Ma (the weighted mean age of the two samples of the Halong granite determined in this study), the calculated εHf(t) values ranged from +10.4 to +15.2 with the T_{DM1} model ages ranging from 610 to 414 Ma and the T_{DM2} model ages ranging from 727 to 423 Ma.

4.2.5. HLG-02

Twelve spots of sample HLG-02 yielded $^{176}Hf/^{177}Hf$ values ranging from 0.28281 to 0.28296 (Table 2). According to the crystallization age of 398 Ma, the calculated εHf(t) values of these spots ranged from +9.9 to +15.1, with the T_{DM1} model ages ranging from 626 to 419 Ma and the T_{DM2} model ages ranging from 760 to 430 Ma.

5. Discussion

5.1. Magmatism in the Chinese Altay

The recent zircon U–Pb dating results for the igneous rocks demonstrate that the magmatism was widespread throughout the Chinese Altay continuously from the early Paleozoic to the early Mesozoic (Han et al., 1997; Chen and Arakawa, 2005; Zhu et al., 2006; Briggs et al., 2007; Yuan et al., 2007; Long et al.,

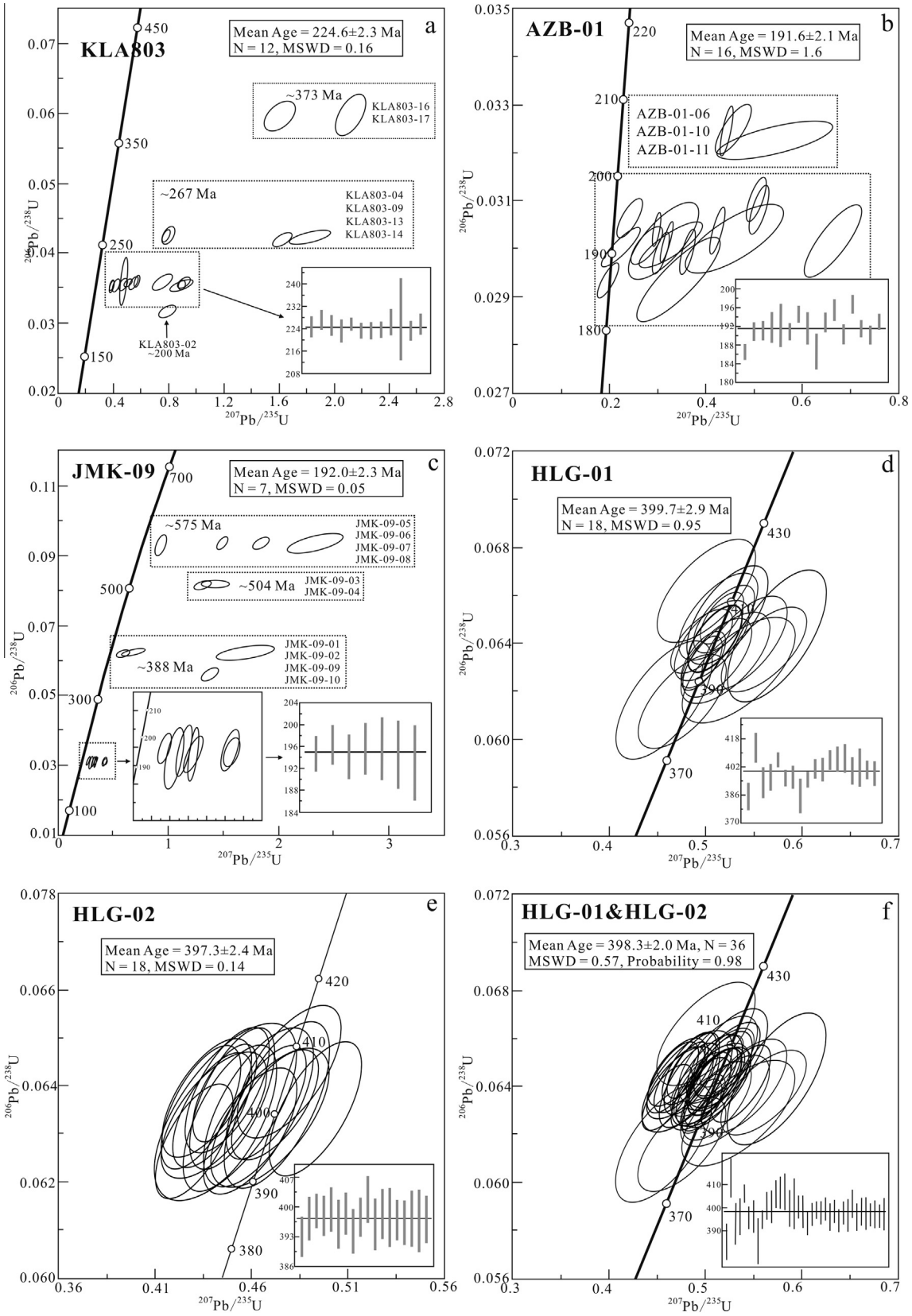

Fig. 5. The U–Pb concordia diagrams of the KLA803 pegmatite, AZB-01 pegmatite, JMK-09 pegmatite and the Halong granite (HLG-01 and HLG-02).

2007; Sun et al., 2008; Cai et al., 2011a,b, 2012; Ren et al., 2011; Lv et al., 2012). The emplacement of the early Paleozoic subduction-related granites in the Chinese Altay was constant and reached a peak in the Devonian (Cai et al., 2011a,b, 2012; Wang et al., 2011), and the post-collision A-type granites and pegmatites mainly appeared after ca. 310 Ma (Zhu et al., 2006; Shen et al.,

Table 2
Hf isotopic compositions of the KLA803 pegmatite, the AZB-01 pegmatite, the JMK-09 pegmatite and the Halong granite (HLG-01 and HLG-02), determined by LA-MC-ICPMS.

Sample	$^{176}Lu/^{177}Hf$	$^{176}Yb/^{177}Hf$	$^{176}Hf/^{177}Hf$	1σ	εHf(*t*)	T_{DM1} (Ma)	T_{DM2} (Ma)
KLA803							
KLA803-01	0.00001	0.00026	0.28268	6	1.1	789	1163
KLA803-02	0.00001	0.00028	0.28265	9	0.1	831	1230
KLA803-03	0.00002	0.00065	0.28271	7	2.2	748	1095
KLA803-04	0.00004	0.00115	0.28268	7	1.1	790	1163
KLA803-05	0.00003	0.00095	0.28270	7	1.8	762	1118
KLA803-06	0.00002	0.00066	0.28263	7	−0.6	858	1275
KLA803-07	0.00004	0.00125	0.28267	7	0.8	804	1185
KLA803-08	0.00004	0.00136	0.28269	7	1.5	776	1141
KLA803-09	0.00006	0.00197	0.28266	9	0.4	818	1208
KLA803-10	0.00001	0.00051	0.28266	7	0.4	817	1208
KLA803-11	0.00002	0.00131	0.28269	8	1.5	776	1140
KLA803-12	0.00003	0.00123	0.28265	8	0.1	831	1230
KLA803-13	0.00004	0.00111	0.28266	9	0.4	817	1208
KLA803-14	0.00003	0.00870	0.28264	7	−0.3	845	1253
KLA803-15	0.00002	0.00253	0.28267	8	0.8	803	1185
AZB-01							
AZB-01-01	0.00001	0.00037	0.28267	5	0.8	803	1185
AZB-01-02	0.00009	0.00309	0.28263	10	−0.6	860	1276
AZB-01-03	0.00050	0.01244	0.28280	8	5.3	632	897
AZB-01-04	0.00010	0.00255	0.28262	11	−1.0	874	1298
AZB-01-05	0.00011	0.00361	0.28272	7	2.5	736	1074
AZB–01–06	0.00001	0.00052	0.28264	7	−0.3	844	1253
AZB-01-07	0.00018	0.00602	0.28276	6	3.9	682	984
AZB-01-08	0.00056	0.01332	0.28278	9	4.6	661	943
AZB-01-09	0.00028	0.00800	0.28272	6	2.5	740	1075
AZB-01-10	0.00095	0.02116	0.28283	7	6.3	597	833
AZB-01-11	0.00014	0.00522	0.28271	6	2.2	751	1096
AZB-01-12	0.00015	0.00409	0.28275	6	3.6	696	1007
AZB-01-13	0.00042	0.00979	0.28274	8	3.2	714	1031
AZB-01-14	0.00081	0.02213	0.28271	7	2.1	764	1102
AZB-01-15	0.00103	0.02321	0.28277	7	4.2	684	969
JMK-09							
JMK-09-01	0.00002	0.00096	0.28272	9	2.6	735	1073
JMK-09-02	0.00001	0.00047	0.28268	6	1.1	789	1163
JMK-09-03	0.00007	0.00348	0.28272	10	2.5	736	1073
JMK-09-04	0.00000	0.00028	0.28270	7	1.8	762	1118
JMK-09-05	0.00000	0.00017	0.28271	7	2.2	748	1095
JMK-09-06	0.00003	0.00163	0.28269	8	1.5	776	1140
JMK-09-07	0.00002	0.00126	0.28267	9	0.8	803	1185
JMK-09-08	0.00006	0.00298	0.28274	8	3.3	708	1028
JMK-09-09	0.00004	0.00226	0.28269	8	1.5	776	1141
JMK-09–10	0.00002	0.00078	0.28266	7	0.4	817	1208
JMK-09-11	0.00002	0.00099	0.28271	7	2.2	748	1095
JMK-09-12	0.00001	0.00064	0.28268	9	1.1	789	1163
JMK-09-13	0.00004	0.00197	0.28270	8	1.8	763	1118
JMK-09-14	0.00003	0.00139	0.28269	9	1.5	776	1140
JMK-09-15	0.00004	0.00222	0.28271	8	2.2	749	1096
HLG-01							
HLG-01-01	0.00113	0.03048	0.28295	10	14.8	429	447
HLG-01-02	0.00138	0.03763	0.28288	10	12.3	533	609
HLG-01-03	0.00103	0.02649	0.28295	12	14.8	428	445
HLG-01-04	0.00104	0.02621	0.28296	7	15.2	414	423
HLG-01-05	0.00042	0.01228	0.28292	9	13.9	463	502
HLG-01-06	0.00182	0.03423	0.2829	9	12.9	510	571
HLG-01-07	0.00172	0.03246	0.28283	9	10.4	610	727
HLG-01-08	0.00128	0.02579	0.28293	8	14.1	460	494
HLG-01-09	0.00147	0.02536	0.28289	10	12.6	520	588
HLG-01-10	0.00142	0.01321	0.28293	8	14	461	497
HLG-01-11	0.00171	0.03222	0.28288	10	12.2	537	615
HLG-02							
HLG-02-01	0.00132	0.03487	0.28294	10	14.4	446	472
HLG-02-02	0.00131	0.0339	0.28291	9	13.3	489	540
HLG-02-03	0.00099	0.02626	0.28281	10	9.9	626	760
HLG-02-04	0.00151	0.04191	0.28296	11	15.1	419	430
HLG-02-05	0.00155	0.04214	0.28293	12	14	463	499
HLG-02-06	0.00118	0.03033	0.28288	9	12.3	530	606
HLG-02-07	0.00109	0.02834	0.28286	9	11.6	557	649
HLG-02-08	0.00107	0.02632	0.28289	10	12.7	514	581
HLG-02-09	0.00167	0.04007	0.28292	11	13.6	479	524

(*continued on next page*)

Table 2 (*continued*)

Sample	$^{176}Lu/^{177}Hf$	$^{176}Yb/^{177}Hf$	$^{176}Hf/^{177}Hf$	1σ	εHf(*t*)	T_{DM1} (Ma)	T_{DM2} (Ma)
HLG-02-10	0.00166	0.04001	0.28294	11	14.3	450	478
HLG-02-11	0.00126	0.03123	0.2829	11	13	502	562
HLG-02-12	0.00118	0.02657	0.28284	10	10.9	587	696

$\varepsilon Hf(t) = \{[(^{176}Hf/^{177}Hf)_S - (^{176}Lu/^{177}Hf)_S \times (e^{\lambda t}-1)]/[(^{176}Hf/^{177}Hf)_{CHUR} - (^{176}Lu/^{177}Hf)_{CHUR} \times (e^{\lambda t}-1)] - 1\} \times 10{,}000$.
$T_{DM1} = 1/\lambda \ln\{[(^{176}Hf/^{177}Hf)_S - (^{176}Hf/^{177}Hf)_{DM}]/[(^{176}Lu/^{177}Hf)_S - (^{176}Lu/^{177}Hf)_{DM}] + 1\}$.
$T_{DM2} = t + 1/\lambda \ln\{[(^{176}Hf/^{177}Hf)_S - (^{176}Hf/^{177}Hf)_{DM}]/[(^{176}Lu/^{177}Hf)_{LC} - (^{176}Lu/^{177}Hf)_{DM}] + 1\}$.
$(^{176}Hf/^{177}Hf)_{DM(0)} = 0.28325$, $(^{176}Lu/^{177}Hf)_{DM(0)} = 0.0384$, $(^{176}Hf/^{177}Hf)_{LC(0)} = 0.282500$, $(^{176}Lu/^{177}Hf)_{LC(0)} = 0.022$, $\lambda = 1.867 \times 10^{-11}$ year^{-1}, *t* = crystallization time of zircon (Griffin et al., 2002; Soderlund et al., 2004).

2011; Lv et al., 2012; Ma, 2014). This prolonged magmatism was closely associated with the tectonic evolution of the Chinese Altay and was transformed from subduction-related to post-collisional, mainly because of the collision between the Siberia and Kazakhstan blocks during the Late Carboniferous and the Early Permian (Chen and Jahn, 2004; Windley et al., 2007; Xiao et al., 2008; Zhou et al., 2008; Cai et al., 2011a,b, 2012; Lv et al., 2012; Zhang and Zhang, 2014).

The zircon U–Pb geochronological studies indicate that the K–A–J pegmatites were emplaced in the Mesozoic and the Halong granite was formed in the middle Paleozoic. They were petrogenetically associated with different tectonic phases of the Chinese Altay and should have formed from different magmas.

5.2. Origin of the magmas of the K–A–J pegmatites and the Halong granite

5.2.1. The K–A–J pegmatites

The εHf(*t*) values of the KLA803 pegmatite, AZB-01 pegmatite and JMK-09 pegmatite ranged from −0.6 to +2.2, from −1.0 to +6.3 and from +0.4 to +3.3, respectively (Table 2). These narrow ranges of εHf(*t*) values of the K–A–J pegmatites indicate that they have formed from closed magmatic systems (Fig. 6a). In the age versus εHf(*t*) diagram, the spots of the samples of the K–A–J pegmatites reside between the DM line and the CHUR line, indicating that the magma source may be a mixture of the depleted mantle and crustal components (Fig. 6a). The T_{DM1} and T_{DM2} model ages of the K–A–J pegmatites vary from 874 to 597 Ma and from 1298 to 833 Ma. In comparison, the Kaluan No. 805 and 806 pegmatites, Kukalagai No. 650 pegmatite, Koktokay No. 3 pegmatite and Kelumute No. 112 pegmatite exhibit negative to low-positive εHf(*t*) values (from 0.0 to +2.5, +0.6 to +2.0, −0.5 to +1.8, +1.3 to +2.4 and +0.0 to +2.4, respectively) but older T_{DM} model ages (1690–1880 Ma, 1747–1851 Ma, 1737–1905 Ma, 1102–1174 Ma and 1112–1225 Ma, respectively; Fig. 6a; Zhu et al., 2006; Chen, 2011; Lv et al., 2012; Ma, 2014), indicating that the magma source of the K–A–J pegmatites may be different from the above-mentioned pegmatites.

5.2.2. The Halong granite

Two samples of the Halong granite yield positive and high εHf(*t*) values from +10.4 to +15.2 and from +9.9 to +15.1. In the age versus εHf(*t*) diagram (Fig. 6a), the spots of samples HLG-01 and HLG-02 reside between the DM line and the CHUR line and are near the DM line, implying a small-scale heterogeneous magma source with a large proportion of the depleted mantle components. The young model ages of the Halong granite (with the T_{DM1} ranging from 626 to 414 Ma and the T_{DM2} ranging from 760 to 423 Ma) indicate that large volumes of juvenile materials have added in its magma source. The previously reported Paleozoic granitoids in the Chinese Altay are characterized by scattered εHf(*t*) values and model ages (ranged from −1.4 to +14.1 and 1680 Ma to 437 Ma, respectively; Cai et al., 2011a,b, 2012; Shen et al., 2011;

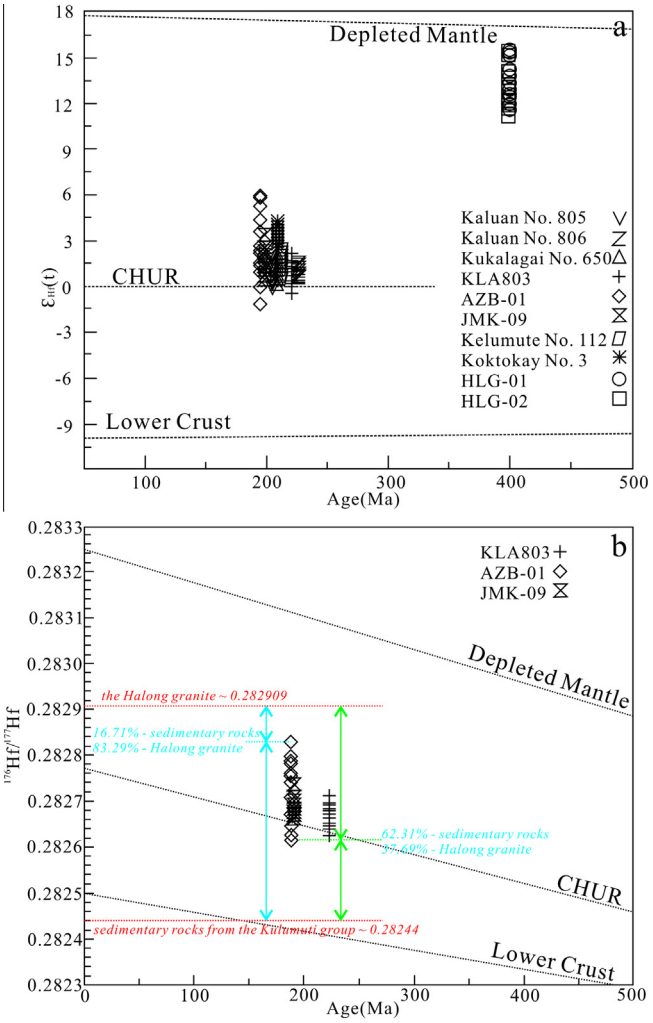

Fig. 6. (a) The age vs. εHf(*t*) diagram of the K–A–J pegmatites and the Halong granite (the Hf isotopic data of the Kaluan No. 805 pegmatite, Kaluan No. 806 pegmatite, Kukalagai No. 650 pegmatite, Kelumute No. 112 pegmatite and Koktokay No. 3 pegmatite are from Chen, 2011; Lv et al., 2012; Ma, 2014); (b) the age vs. $^{176}Hf/^{177}Hf$ diagram of the K–A–J pegmatites, where the average $^{176}Hf/^{177}Hf$ ratio (0.282909) of the Halong granite is calculated on the basis of our data in this work (avg. $^{176}Hf/^{177}Hf = 0.282905$, avg. $^{176}Lu/^{177}Hf = 0.001314$, $N = 23$), and the average $^{176}Hf/^{177}Hf$ ratio (0.28244) of the sediments from the Kulumuti group is calculated from the εNd(*t*) value (−3.5, Wang et al., 2014), the $^{176}Lu/^{177}Hf$ ratio (0.015, avg. Crust, Han and Ma, 2003) and a formula of εHf = 1.83εNd + 0.60 (Vervoort et al., 1999).

Wang et al., 2011), and they have been interpreted by an early-middle Paleozoic subduction model and a late Paleozoic post-collision model (Cai et al., 2011b; Shen et al., 2011). According to a subduction-related magmatism (Nicholls and Ringwood, 1972; Kay, 1980; Wyllie and Sekine, 1982; Hofmann, 1997; Ishizuka et al., 2003), the Halong granite was probably derived from the

partial melting of juvenile materials with a slight involvement of crustal materials. In addition, the differences in εHf(t) values and model ages demonstrate that the Halong granite was not the parental granite of the K–A–J pegmatites.

5.3. Components of the initial magmas of the K–A–J pegmatites

5.3.1. The mixing model for two end members of A and B

The atomic concentrations of Hf isotopes (^{176}Hf and ^{177}Hf) of a sample associated with a two-end mixed magma can be presented as

$$^{176}Hf_S = \frac{Hf_A}{W_{176}}\,^{176}Hf_A Nf + \frac{Hf_B}{W_{176}}\,^{176}Hf_B N(1-f) \quad (1)$$

$$^{177}Hf_S = \frac{Hf_A}{W_{177}}\,^{177}Hf_A Nf + \frac{Hf_B}{W_{177}}\,^{177}Hf_B N(1-f) \quad (2)$$

where Hf_A and Hf_B are the abundances of Hf in the end members of A and B, W is the relative atomic mass (the molar mass), N is the Avogadro constant, and f is the mixing ratio. $^{177}Hf_A$, $^{177}Hf_B$, $^{176}Hf_A$ and $^{176}Hf_B$ are the Hf isotopic abundances in the end members A and B. Dividing Eq. (1) by Eq. (2), the Hf isotopic ratio can be expressed as

$$\left(^{176}Hf/^{177}Hf\right)_S = \frac{\frac{Hf_A}{W_{176}}\,^{176}Hf_A Nf + \frac{Hf_B}{W_{176}}\,^{176}Hf_B N(1-f)}{\frac{Hf_A}{W_{177}}\,^{177}Hf_A Nf + \frac{Hf_B}{W_{177}}\,^{177}Hf_B N(1-f)} \quad (3)$$

where $W_{176}/W_{177} = 176/177 \approx 1$, and $^{177}Hf_A$ is approximately equal to $^{177}Hf_B$ because ^{177}Hf is a stable isotope. Eq. (3) can therefore be simplified as follows:

$$\left(^{176}Hf/^{177}Hf\right)_S = \frac{Hf_A f}{Hf_A f + Hf_B(1-f)}\left(^{176}Hf/^{177}Hf\right)_A + \frac{Hf_B(1-f)}{Hf_A f + Hf_B(1-f)}\left(^{176}Hf/^{177}Hf\right)_B \quad (4)$$

This is the Hf isotopic mixing equation of a sample with two end members (A and B).

5.3.2. The components of the initial magma of the K–A–J pegmatites

Liu et al. (2012) suggested that the source components of granitoids and volcanic rocks from the Chinese Altay included continental-crust component, asthenospheric mantle and juvenile source. Because juvenile materials commonly contribute to arc and syn-collision magmatism (Kovalenko et al., 2004; Cai et al., 2010), and the K–A–J pegmatites were probably formed from a post-collisional magmatism that is featured by intensive crust-mantle interactions (see Section 5.4), we accordingly have selected the Lower Crust (LC) and the Depleted Mantle (DM) as the mixing end-members of the initial magma. The Hf isotopic ratio of a sample can be presented as

$$\left(^{176}Hf/^{177}Hf\right)_S = \frac{Hf_{DM} f}{Hf_{DM} f + Hf_{LC}(1-f)}\left(^{176}Hf/^{177}Hf\right)_{DM} + \frac{Hf_{LC}(1-f)}{Hf_{DM} f + Hf_{LC}(1-f)}\left(^{176}Hf/^{177}Hf\right)_{LC} \quad (5)$$

where $(^{176}Hf/^{177}Hf)_{DM} = 0.283250$, $(^{176}Lu/^{177}Hf)_{DM} = 0.038400$, $(^{176}Hf/^{177}Hf)_{LC} = 0.282500$, $(^{176}Lu/^{177}Hf)_{LC} = 0.022$, $Hf_{DM} = 0.167$ μg/g and $Hf_{LC} = 2.10$ μg/g (Wedepohl, 1995).

By utilizing the substitution method, the mixing ratios (f) of the K–A–J pegmatites can be calculated as ranging from 0.72 to 0.91, indicating that the initial magma of the K–A–J pegmatites was possibly composed of 72–91 wt.% depleted mantle components and 9–28 wt.% lower crust components.

Fundamentally because the abundance of Hf in the Depleted Mantle (0.167 μg/g) is much lower than that in the Lower Crust (2.1 μg/g), large amounts of mantle materials (72–91 wt.%) should have been added into the initial magma of the K–A–J pegmatites to elevate the $^{176}Hf/^{177}Hf$ ratios. However, the geochemical and mineralogical characteristics of LCT-type pegmatites exhibit appreciable continental crust affinities (Černý, 1991; Shelley, 1993; London, 2008). Such large proportions of mantle contributions are obviously in contradiction with the definition of the LCT-type pegmatite, indicating that this mixing model for the initial magma of the K–A–J pegmatites is impractical.

Recent studies show that the detrital zircons from the early Paleozoic sedimentary rocks of the Kulumuti group in the Chinese Altay were dominantly formed between 430 and 580 Ma and 750 and 950 Ma with only a minor population of Meso- to Paleoproterozoic grains (Wang et al., 2014). As featured by the negative initial εNd(t) values from −4.3 to −0.2 and the old T_{DM} model ages between 1.22 and 1.56 Ga, these sedimentary rocks are considered to be derived from a near source dominated by the early Paleozoic igneous material deposited after the Middle Ordovician (Wang et al., 2014). Being the country rocks of the Halong granite, the sedimentary rocks from the Kulumuti group may serve as another possible magma source for the K–A–J pegmatites. From the Hf isotopic features, the remelting of the Halong granite could produce melts characterized by high positive εHf(t) values (from +9.9 to +15.2) and young model ages (T_{DM}) (with the T_{DM1} from 626 to 414 Ma and the T_{DM2} from 760 to 423 Ma). After mingling with the sedimentary rocks from the Kulumuti group, the εHf(t) values and the model ages of the mixed magma would become lower and older. For this magma source, the geochemical characteristics of the pegmatites are controlled by the proportions of these two components.

The Hf isotopic ratio of a sample can be reported as

$$\left(^{176}Hf/^{177}Hf\right)_S = \frac{Hf_{HL} f}{Hf_{HL} f + Hf_{SD}(1-f)}\left(^{176}Hf/^{177}Hf\right)_{HL} + \frac{Hf_{SD}(1-f)}{Hf_{HL} f + Hf_{SD}(1-f)}\left(^{176}Hf/^{177}Hf\right)_{SD} \quad (6)$$

where $Hf_{HL} \approx Hf_{SD} = 4$ μg/g (Han and Ma, 2003; Ma, 2014). Eq. (6) can be simplified as

$$\left(^{176}Hf/^{177}Hf\right)_S = f\left(^{176}Hf/^{177}Hf\right)_{HL} + (1-f)\left(^{176}Hf/^{177}Hf\right)_{SD} \quad (7)$$

which is applicable to the Lever Rule.

The Lever Rule is a tool widely used to determine the weight percentages of each phase of a binary equilibrium phase diagram (Smith and Hashemi, 2006). To quantifiably characterize the weight percentage of each mixed component for the initial magma of the pegmatites in a more convenient way, we first introduce the Lever Rule into Hf isotopic system. The $^{176}Hf/^{177}Hf$ isotopic ratios of the Halong granite and the sedimentary rocks from the Kulumuti group may serve as two end members of the lever, and the $^{176}Hf/^{177}Hf$ isotopic ratio of a sample can be considered as the pivot. This allows the Lever Rule to be functional when calculating the weight percentages in the age versus $^{176}Hf/^{177}Hf$ diagram. As shown in Fig. 6b, the initial magma of the K–A–J pegmatites was probably composed of 38–83 wt.% Halong granite and 17–62 wt.% sedimentary rocks from the Kulumuti group.

Here, if and only if $Hf_A \approx Hf_B$, the Hf isotopic mixing Eq. (4) can be simplified as

$$\left(^{176}Hf/^{177}Hf\right)_S = f\left(^{176}Hf/^{177}Hf\right)_A + (1-f)\left(^{176}Hf/^{177}Hf\right)_B \quad (8)$$

which is suitable for the Lever Rule in the age versus $^{176}Hf/^{177}Hf$ diagram. This method can be used to quantify the weight percentages of the components of a two-end mixed magma and would bring great benefits to further geochemical studies.

5.4. Petrogenesis of the K–A–J pegmatites

To satisfy the increasing demands for rare-metal exploitation, the petrogenetic studies of the pegmatites in the Chinese Altay have attracted a substantial amount of attentions in recent years (Fig. 1, Zhu et al., 2006; Wang et al., 2007; Ren et al., 2011; Lv et al., 2012; Ma, 2014). The emplacement ages of more than 40 pegmatite veins have been ascertained from 280 Ma to 180 Ma using zircon U–Pb dating (Zhu et al., 2006; Wang et al., 2007; Ren et al., 2011; Lv et al., 2012; Ma, 2014). Additionally, the distributions of these pegmatites show temporal and spatial regularities: the Permian pegmatites were only exposed in Terrane 4; the Triassic pegmatites occurred in a wide range of Terranes 2, 3 and 4; and the Jurassic pegmatites mainly appeared in Terrane 3 (Fig. 1).

Rare-element pegmatites are petrogenetically associated with two types of tectonic settings: post-collision zones and intracontinental rifts (Vladimirov et al., 1998, 2013; Altukhov et al., 2005; Martin and De Vito, 2005; Tkachev, 2011; Gusev et al., 2012; Zagorsky et al., 2015). Currently, the Chinese Altay is widely accepted to have been dominated by a post-collision tectonic setting during the Late Carboniferous and the Mesozoic (Han et al., 1997; Chen and Jahn, 2004; Zhang and Zhang, 2014). Commonly cited trigger for post-collision magmatism is delamination or thinning of the lithospheric mantle beneath the over-riding plate (Pearce et al., 1990; Turner et al., 1992; Kay and Kay, 1993), and the subsequent upwelling of asthenosphere could induce the partial melting of the lower crust or even the middle crust accompanying a large-scale mantle-crustal interaction (Bird, 1979; Houseman et al., 1981; Liégeois et al., 1998; Bonin, 2004; Duggen et al., 2005; Zhao et al., 2007). In accordance with the post-collision magmatism, the petrogenesis of the K–A–J pegmatites can be summarized as the following multi-stage processes (Model 1): (1) the lower crustal materials were heated by the upwelling hot asthenosphere and melted partially in a post-collision extensional tectonic setting; (2) the crust-derived magma mixed with the mantle-derived magma at the deep crust; (3) the mixed magma moved upward though the extensional fractures and was stored at the shallow crust in a magma chamber; (4) after a long time of fractional crystallization in the magma chamber, the highly evolved felsic magma (the residual melt) intruded into the Late Silurian sedimentary rocks (the Kulumuti group) and then crystallized to form the pegmatites.

In Model 1, the excessively high weight percentages (72–91 wt.%) of the depleted mantle components in the initial magma of the K–A–J pegmatites indicate that this model is unrealistic. Therefore, we establish a new model (Model 2): (1) because of the upwelling of the asthenosphere in a post-collision extensional setting, the decompression and added heat induced the partial melting of the Halong granite and the surrounding sedimentary rocks from the Kulumuti group at the lower crust, or even at the middle curst; (2) the felsic magma moved upward through the extensional fractures and then crystallized to become pegmatites at the shallow crust (Fig. 7).

In the Chinese Altay, a significant question has puzzled geological workers and geologists for a long time, that is, whether the pegmatites have parental granites. The Jideke granite, a possible parental granite, has been recently dated between 445.6 ± 4.3 and 455.6 ± 5.4 Ma with zircon U–Pb geochronology and been concluded as a barren granite because its emplacement age is much older than the Kelumute No. 112 pegmatites (Lv et al., 2012). By contrast, Liu et al. (2014) determined the zircon U–Pb age of the Aral granite at 211.4 ± 0.8 Ma using LA-MC-ICP-MS methods, similar to the molybdenite Re–Os isochron age of 208.9 Ma from the Koktokay No. 3 pegmatite, and they therefore assumed that this pegmatite was derived from the Aral granite. However, the geochronological results could make little sense of the petrogenetic relationships without detailed studies of the evolutionary processes or sufficient support from isotopic data. In addition, the K-feldspar of the Aral granite exhibits low Rb and Cs contents (from 454.83 to 666.03 ppm and from 2.42 to 6.26 ppm) and high K/Rb ratios (from 167 to 246), indicating that this granite is a barren granite and is unlikely to be the parental granite of the Koktokay No. 3 pegmatite (Liu, 2013). Therefore, questions remain regarding (1) whether the pegmatite requires a parental granite, and (2) the location (when identified as existing) of the parental granite.

Even though Model 1 is a conventional model for interpreting post-collision magmatism (Bird, 1979; Houseman et al., 1981; Liégeois et al., 1998; Bonin, 2004; Duggen et al., 2005; Zhao et al., 2007), there is also a vital problem in addition to the contradiction from the calculated results, that is, how the mixed magma develops to be a highly evolved felsic magma. According to this issue, a magma chamber is necessary for Model 1 to allow the magma to experience a high degree of fractional crystallization. However, until now, no single granite has been ascertained to be the parental granite for the K–A–J pegmatites in the Chinese Altay (Lv et al., 2012; Ma, 2014). Therefore, it is reasonable to propose a new petrogenetic model. Partial melting of pre-existing granites is an acceptable mechanism for generating felsic melts (Collins et al., 1982; Clemens et al., 1986; Anderson and Morrison, 1992; Skjerlie and Johnston, 1993; King et al., 1997). In combination with the

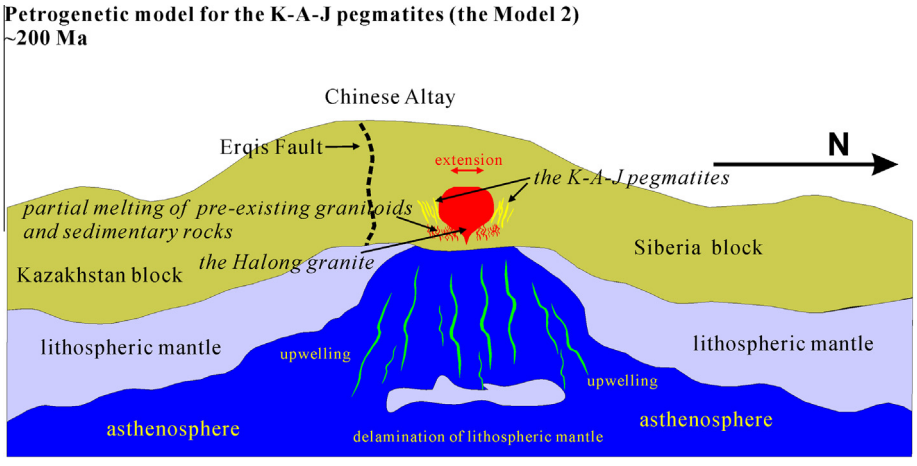

Fig. 7. Sketch map of the petrogenetic model of the K–A–J pegmatites (the post-collision tectonic setting is modified after Shen et al., 2011 and Cai et al., 2012).

spatial relationships, the Hf isotopic characteristics, and the calculated results of the components of the initial magmas, we suggest that Model 2 is more rational for interpreting the petrogenesis of the K–A–J pegmatites.

6. Conclusions

Based on the zircon U–Pb geochronological and Hf isotopic studies of the KLA803 pegmatite, AZB-01 pegmatite, JMK-09 pegmatite and the Halong granite, the following conclusions can be drawn:

(1) The K–A–J pegmatites from the KAQ ore fields were emplaced in the Mesozoic, and the Halong granite was formed in the middle Paleozoic.
(2) The K–A–J pegmatites probably originated from a mixed source that was composed of 72–91 wt.% depleted mantle components and 9–28 wt.% lower crust components or of 38–83 wt.% Halong granite and 17–62 wt.% sedimentary rocks from the Kulumuti group, and the Halong granite was likely derived from the partial melting of juvenile materials with a slight involvement of crustal materials.
(3) The large emplacement age gaps and different Hf isotopic compositions between the K–A–J pegmatites and the Halong granite indicate that they have formed from different magmas and the Halong granite is not the parental granite of the K–A–J pegmatites.
(4) The Model 2, referring to that the K–A–J pegmatites originated from the partial melting of the Halong granite and the sedimentary rocks from the Kulumuti group without a parental granite, is a new petrogenetic model for the pegmatites in the Chinese Altay, which requires further verification and consolidation.

Acknowledgements

We thank the editors and the reviewers very much for their constructive comments that have greatly improved the manuscript. This study was jointly supported by the National Basic Research Program of China (973 Program) (No. 2007CB411303), the National Supporting Program of China (305 Program) (No. 2007BAB25B01), and the National Science Foundation of China under Grant 41073051.

References

Altukhov, E.N., Altukhov, E.E., Vashurin, A.I., Usova, T.Yu., 2005. Fundamentals of Rare-Metal Metallogeny. IMGRE, Moscow, pp. 1–20 (in Russian).
Amelin, Y., Lee, D.C., Halliday, A.N., 2000. Early-Middle Archean crustal evolution deduced from Lu–Hf and U–Pb isotopic studies of single zircon grains. Geochim. Cosmochim. Acta 64, 4205–4225.
Anderson, J.L., Morrison, J., 1992. The role of anorogenic granites in the Proterozoic crustal development of North America. Develop. Precambrian Geol. 10, 263–299.
Badarch, G., Cunningham, W.D., Windley, B.F., 2002. A new terrane subdivision for Mongolia: implications for the Phanerozoic crustal growth of Central Asia. J. Asian Earth Sci. 21, 87–110.
Baijot, M., Hatert, F., Philippo, S., 2012. Mineralogy and geochemistry of phosphates and silicates in the Sapucaia pegmatite, Minas Gerais, Brazil: genetic implications. Can. Mineral. 50, 1531–1554.
BGMRX (Bureau of Geology Mineral Resources of Xinjiang Uygur Autonomous Region), 1993. Regional Geology of Xinjiang Uygur Autonomous Region. People's Republic of China, Ministry of Geology and Mineral Resources. Geological Memoirs, Series 1, No. 32. Geological Publishing House, Beijing, pp. 6–206 (in Chinese).
Bird, P., 1979. Continental delamination and the Colorado Plateau. J. Geophys. Res. 84, 7561–7571.
Biske, Y.S., Seltmann, R., 2010. Paleozoic Tian-shan as a transitional region between the Rheic and Urals-Turkestan Oceans. Gondwana Res. 17, 602–613.
Black, L.P., Kamo, S.L., Allen, C.M., Aleinikoff, J.N., Davis, D.W., Korsch, R.J., Foudoulis, C., 2003. TEMORA 1: a new zircon standard for Phanerozoic U–Pb geochronology. Chem. Geol. 200, 155–170.
Bonin, B., 2004. Do coeval mafic and felsic magmas in post-collisional to within-plate regimes necessarily imply two contrasting, mantle and crustal, sources? A review. Lithos 78, 1–24.
Briggs, S.M., Yin, A., Manning, C.E., Chen, Z.L., Wang, X.F., Grove, M., 2007. Late Paleozoic tectonic history of the Ertix fault in the Chinese Altai and its implications for the development of the Central Asian Orogenic System. Geol. Soc. Am. Bull. 119, 944–960.
Briggs, S.M., Yin, A., Manning, C.E., Chen, Z.L., Wang, X.F., 2009. Tectonic development of the southern Chinese Altai Range as determined by structural geology, thermobarometry, $^{40}Ar/^{39}Ar$ thermochronology, and Th/Pb ion-microprobe monazite geochronology. Geol. Soc. Am. Bull. 121, 1381–1393.
Burnham, C.W., Ohmoto, H., 1980. Late stage processes of felsic magmatism. Min. Geol. Special Issue 8, 1–11.
Cai, K., Sun, M., Yuan, C., Zhao, G., Xiao, W., Long, X., Wu, F., 2010. Geochronological and geochemical study of mafic dykes from the northwest Chinese Altai: implications for petrogenesis and tectonic evolution. Gondwana Res. 18, 638–652.
Cai, K., Sun, M., Yuan, C., Zhao, G., Xiao, W., Long, X., Wu, F., 2011a. Geochronology, petrogenesis and tectonic significance of peraluminous granites from the Chinese Altai, NW China. Lithos 127, 261–281.
Cai, K., Sun, M., Yuan, C., Zhao, G., Xiao, W., Long, X., Wu, F., 2011b. Prolonged magmatism, juvenile nature and tectonic evolution of the Chinese Altai, NW China: evidence from zircon U–Pb and Hf isotopic study of Paleozoic granitoids. J. Asian Earth Sci. 42, 949–968.
Cai, K., Sun, M., Yuan, C., Long, X., Xiao, W., 2011c. Geological framework and Paleozoic tectonic history of the Chinese Altai, NW China: a review. Russ. Geol. Geophys. 52, 1619–1633.
Cai, K., Sun, M., Yuan, C., Xiao, W.J., Zhao, G.C., Long, X.P., Wu, F.Y., 2012. Carboniferous mantle-derived felsic intrusion in the Chinese Altai, NW China: implications for geodynamic change of the accretionary orogenic belt. Gondwana Res. 22, 681–698.
Černý, P., 1991. Rare element granitic pegmatites. Part I: anatomy and internal evolution of pegmatite deposits. Geosci. Can. 18, 49–67.
Černý, P., Corkery, M.T., Halden, N.M., Ferreira, K., Brisbin, W.C., Chackowsky, L.E., Meintzer, R.E., Longstaffe, F.J., Trueman, D.L., 2012. Extreme fractionation and deformation of the leucogranite–pegmatite suite at Red Cross Lake, Manitoba, Canada. I. Geological setting. Can. Mineral. 50, 1793–1806.
Cherniak, D.J., Watson, E.B., 2003. Diffusion in zircon. Rev. Mineral. Geochem. 53 (1), 113–143.
Chen, B., Arakawa, Y., 2005. Elemental and Nd–Sr isotopic geochemistry of granitoids from the West Junggar foldbelt (NW China), with implications for Phanerozoic continental growth. Geochim. Cosmochim. Acta 69, 1307–1320.
Chen, B., Jahn, B.M., 2002. Geochemical and isotopic studies of the sedimentary and granitic rocks of the Altai orogen of NW China and their tectonic implications. Geol. Mag. 139, 1–13.
Chen, B., Jahn, B.M., 2004. Genesis of post-collisional granitoids and basement nature of the Junggar Terrane, NW China: Nd–Sr isotope and trace element evidence. J. Asian Earth Sci. 23, 69–703.
Chen, J.F., 2011. Geochemistry of the plate part in Altai No. 3 pegmatite and its formation and evolution. A Dissertation Submitted to Graduate University of Chinese Academy of Sciences for the Degree of Master of Philosophy, pp. 1–86.
Clemens, J.D., Holloway, J.R., White, A.J.R., 1986. Origin of an A-type granite: experimental constraints. Am. Mineral. 71, 317–324.
Collins, W.J., Beams, S.D., White, A.J.R., Chappell, B.W., 1982. Nature and origin of A-type granites with particular reference to southeastern Australia. Contrib. Miner. Petrol. 80, 189–200.
Corfu, F., Hanchar, J.M., Hoskin, P.W.O., Kinny, P., 2003. Atlas of zircon textures. Rev. Mineral. Geochem. 53, 469–500.
Duggen, S., Hoernle, K., Bogaard, P.V., Garbe-Schönberg, D., 2005. Post-collisional transition from subduction- to intraplate-type magmatism in the westernmost Mediterranean: evidence for continental-edge delamination of subcontinental lithosphere. J. Petrol. 46, 1155–1201.
Fuertes-Fuente, M., Martin-Izard, A., Boiron, M.C., Vinuela, J.M., 2000. P–T path and fluid evolution in the Franqueira granitic pegmatite, central Galicia, northwestern Spain. Can. Mineral. 38, 1163–1175.
Goolaerts, A., Mattielli, N., de Jong, J., Weis, D., Scoates, J.S., 2004. Hf and Lu isotopic reference values for the zircon standard 91500 by MC-ICP-MS. Chem. Geol. 206, 1–9.
Griffin, W.L., Wang, X.M., Jacksion, S.E., Pearson, N.J., O'Reilly, S.Y., Xu, X.S., Zhou, X. M., 2002. Zircon chemistry and magma mixing, SE China: in-suit analysis of Hf isotopes, Tonglu and Pingtan igneous complexes. Lithos 61, 237–269.
Goad, B.E., Černý, P., 1981. Peraluminous pegmatitic granites and their pegmatite aureoles in the Winnipeg River District, Southeastern Manitoba. Can. Mineral. 19, 177–194.
Gusev, G.S., Gushchin, A.V., Mezhelovskiy, N.V., Kilipko, V.A., 2012. Two types of rare metal mineralization in territory of Russia: geodynamic models of forming. Razvedka i Okhrana Nedr 2, 38–42.
Han, B.F., Wang, S.G., Jahn, B.M., Hong, D.W., Kagami, H., Sun, Y.L., 1997. Depletedmantle source for the Ulungur River A-type granites from North Xinjiang, China: geochemistry and Nd–Sr isotopic evidence, and implications for Phanerozoic crustal growth. Chem. Geol. 138, 135–159.
Han, Y.W., Ma, Z.D., 2003. Geochemistry. Geological Publishing House, pp. 1–370.
Hanchar, J.M., Hoskin, P.W.O., 2003. Zircon. Rev. Miner. Geochem. 53, 1–500.

Hawkesworth, C.J., Kemp, A.I.S., 2006. Using hafnium and oxygen isotopes in zircons to unravel the record of crustal evolution. Chem. Geol. 226 (3), 144–162.
Hofmann, A.W., 1997. Mantle geochemistry: the message from oceanic volcanism. Nature 385, 219–229.
Hoskin, P.W.O., Schaltegger, U., 2003. The composition of zircon and igneous and metamorphic petrogenesis. Rev. Mineral. Geochem. 53 (1), 27–62.
Houseman, G., McKenzie, D., Molnar, P., 1981. Convective instability of a thickened boundary layer and its relevance for the thermal evolution of continental convergent belts. J. Geophys. Res. 86, 6115–6132.
Hulsbosch, N., Hertogen, J., Dewaele, S., Andre, L., Muchez, P., 2014. Alkali metal and rare earth element evolution of rock-forming minerals from the Gatumba area pegmatites (Rwanda): quantitative assessment of crystal-melt fractionation in the regional zonation of pegmatite groups. Geochim. Cosmochim. Acta 132, 349–374.
Ishizuka, O., Taylor, R.N., Milton, J.A., Nesbitt, R.W., 2003. Fluid–mantle interaction in an intra-oceanic arc: constraints from high-precision Pb isotopes. Earth Planet. Sci. Lett. 211, 221–236.
Jahns, R.H., Burnham, C.W., 1969. Experimental studies of pegmatite genesis: a model for the derivation and crystallization of granitic pegmatites. Econ. Geol. 64, 843–864.
Jahn, B.M., Wu, F.Y., Chen, B., 2000. Massive granitoid generation in central Asia: Nd isotopic evidence and implication for continental growth in the Phanerozoic. Episodes 23, 82–91.
Jolliff, B.L., Papike, J.J., Shearer, C.K., 1992. Petrogenetic relationships between pegmatite and granite based on geochemistry of muscovite in pegmatite wall zones, Black Hills, South Dakota, USA. Geochim. Cosmochim. Acta 56, 1915–1939.
Kay, R.W., 1980. Implication of a melting-mixing model for element recycling in the crust–upper mantle system. J. Geol. 88, 497–522.
Kay, R.W., Kay, S.M., 1993. Delamination and delamination magmatism. Tectonophysics 219, 177–189.
King, P.L., White, A.J.R., Chappell, B.W., Allen, C.M., 1997. Characterization and origin of aluminous A-type granites from the Lachlan Fold Belt, southeastern Australia. J. Petrol. 38, 371–391.
Kinny, P.D., Maas, R., 2003. Lu–Hf and Sm–Nd isotope systems in zircon. Rev. Mineral. Geochem. 53 (1), 327–341.
Kovalenko, V.I., Yarmolyuk, V.V., Kovach, V.P., Kotov, A.B., Kozakov, I.K., Salnikova, E. B., Larin, A.M., 2004. Isotope provinces, mechanisms of generation and sources of the continental crust in the Central Asian mobile belt: geological and isotopic evidence. J. Asian Earth Sci. 23 (5), 605–627.
Laurent-Charvet, S., Charvet, J., Monie', P., Shu, L., 2003. Late Paleozoic strike-slip shear zones in eastern central Asia (NW China): new structural and geochronological data. Tectonics 22, 1009.
Lira, R., Gallinsky, M.A., Bernard, F., Roquet, M.B., 2012. The intragranitic Potrerillos NYF pegmatites and their A-type host granites of the Las Chacras-Potrerillos batholith, Sierra de San Luis, Argentina. Can. Mineral. 50, 1729–1750.
Liégeois, J.P., Navez, J., Hertogen, J., Black, R., 1998. Contrasting origin of post-collisional high-K calc-alkaline and shoshonitic versus alkaline and peralkaline granitoids. The use of sliding normalization. Lithos 45, 1–28.
Lima, S.M., Neiva, A.M.R., Ramos, J.M.F., Cuesta, A., 2014. Long-lived magmatic systems and implications on the recognition of granite–pegmatite genetic relations: characterization of the Pavia granitic pegmatites (Ossa-Morena Zone, Portugal). Chem. Erde 74, 625–639.
Liu, H., 2013. Geochemical study on petrogenesis of Aral granite and the Keketuohai No. 3 pegmatite vein, Altay Xinjiang. A Dissertation Submitted to the Kunming University of Science and Technology for the Degree of Master of Philosophy, pp. 1–62.
Liu, W., Liu, X.J., Xiao, W.J., 2012. Massive granitoid production without massive continental-crust growth in the Chinese Altay; insight into the source rock of granitoids using integrated zircon U–Pb age, Hf–Nd–Sr isotopes and; geochemistry. Am. J. Sci. 312, 629–684.
London, D., 1986. The magmatic–hydrothermal transition in the Tanco rare-element pegmatite: evidence from fluid inclusions and phase equilibrium experiments. Am. Mineral. 71, 376–395.
London, D., 1990. Internal differentiation of rare-element pegmatites: a synthesis of recent research. GSA Special Paper 246, pp. 35–50.
London, D., 2005. Granitic pegmatites: an assessment of current concepts and directions for the future. Lithos 80, 281–303.
London, D., 2008. Pegmatites: The Canadian Mineralogist Special Publication 10, p. 347.
Long, X.P., Sun, M., Yuan, C., Xiao, W.J., Lin, S.F., Wu, F.Y., Xia, X.P., Cai, K.D., 2007. U–Pb and Hf isotopic study of zircons from metasedimentary rocks in the Chinese Altai: implications for Early Palaeozoic tectonic evolution. Tectonics 26, TC5015.
Long, X.P., Sun, M., Yuan, C., Xiao, W.J., Cai, K.D., 2008. Early Paleozoic sedimentary record of the Chinese Altai: implications for its tectonic evolution. Sed. Geol. 208 (3–4), 88–100.
Long, X.P., Yuan, C., Sun, M., Xiao, W.J., Zhao, G.C., Wang, Y.J., Cai, K.D., 2010. Detrital zircon ages and Hf isotopes of the early Paleozoic Flysch sequence in the Chinese Altai, NW China: new constraints on depositional age, provenance and tectonic evolution. Tectonophysics 180, 213–231.
Ludwig, K.R., 2003. User's manual for Isoplot/Ex, Version 3. 00. A Geochronological Toolkit for Microsoft Excel. Berkeley Geochronology Center Special Publication 4, pp. 1–70.
Lv, Z.H., Zhang, H., Tang, Y., Guan, S.J., 2012. Petrogenesis and magmatic hydrothermal evolution time limitation of Kelumute No. 112 pegmatite in Altay, Northwestern China: evidence from zircon U–Pb and Hf isotopes. Lithos 154, 374–391.
Martin, R.F., De Vito, C., 2005. The patterns of enrichment in felsic pegmatites ultimately depend on tectonic setting. Can. Mineral. 43 (6), 2027–2048.
Ma, Z.L., 2014. Zircon U–Pb dating and Hf isotopes of pegmatites from the Kaluan mining area in the Altay, Xinjiang and their genetic relationship with the Halong granite. A Dissertation Submitted to Graduate University of Chinese Academy of Sciences for the Degree of Master of Philosophy, pp. 1–70.
Morgan VI, G.B., London, D., 1999. Crystallization of the little three layered pegmatite–aplite dike, Ramona District, California. Contrib. Miner. Petrol. 136, 310–330.
Neiva, A.M.R., Gomes, M.E.P., Ramos, J.M.F., Silva, P.B., 2008. Geochemistry of granitic aplite–pegmatite sills and their minerals from Arcozelo da Serra (Gouveia, central Portugal). Eur. J. Mineral. 20, 465–485.
Neiva, A.M.R., Silva, P.B., Ramos, J.M.F., 2012. Geochemistry of granitic aplite–pegmatite veins and sills and their minerals from the Sabugal area, central Portugal. Neues Jahrbuch für Mineralogie-Abhandlungen 189, 49–74.
Nicholls, I.A., Ringwood, A.E., 1972. Production of silica-saturated magmas in island arcs. Earth Planet. Sci. Lett. 17, 243–246.
Norton, J.J., 1983. Sequence of mineral assemblages in differentiated granitic pegmatites. Econ. Geol. 78, 854–874.
Pearce, J.A., Bender, J.F., Delong, S.E., Kidd, W.S.F., Low, P.J., Guner, Y., Sargolu, F., Yilmaz, Y., Moorbath, S., Mitchell, J.G., 1990. Genesis of collision volcanism in eastern Anatolia, Turkey. J. Volcanol. Geoth. Res. 44, 189–229.
Pearce, N.J.G., Perkins, W.T., Westgate, J.A., Gorton, M.P., Jackson, S.E., Neal, C.R., Chenery, S.P., 1997. A compilation of new and published major and trace element data for NIST SRM 610 and NIST SRM 612 glass reference materials. Geostandard Newslett. 21, 115–144.
Ren, B.Q., Zhang, H., Tang, Y., Lv, Z.H., 2011. LA-ICPMS U–Pb zircon geochronology of the Altai pegmatites and its geological significance. Acta Mineral. Sin. 31, 587–596 (in Chinese with English abstract).
Roda-Robles, E., Pesquera, A., Gil-Crespo, P.P., 2012. The Puentemocha berylphosphate granitic pegmatite, Salamanca, Spain: internal structure, petrography and mineralogy. Can. Mineral. 50, 1573–1587.
Rubatto, D., Gebauer, D., 2000. Use of cathodoluminescence for U–Pb zircon dating by IOM Microprobe: some examples from the western Alps. In: Pagel, M. (Ed.), Cathodoluminescence in Geoscience. Springer-Verlag, Berlin Heidelberg, pp. 373–400.
Scherer, E.E., Cameron, K.L., Blichert-Toft, J., 2000. Lu–Hf garnet geochronology: closure temperature relative to the Sm–Nd system and the effects of trace mineral inclusions. Geochim. Cosmochim. Acta 64, 3413–3432.
Selway, J.B., Breaks, F.W., 2006. A review of rare-element (Li–Cs–Ta) pegmatite exploration techniques for the Superior Province, Canada, and large world tantalum deposits. Explor. Min. Geol. 14, 1–30.
Sengör, A.M.C., Natalin, B.A., Burtman, V.S., 1993. Evolution of the Altaid tectonic collage and Paleozoic crustal growth in Eurasia. Nature 364, 299–307.
Sengör, A.M.C., Natalin, B.A., 1996. Turkic-type orogeny and its role in the making of the continental crust. Annu. Rev. Earth Planet. Sci. 24, 263–337.
Smith, William F, Hashemi, J., 2006. Foundations of Materials Science and Engineering, fourth ed. McGraw-Hill, pp. 318–320.
Shearer, C.K., Papike, J.J., Jolliff, B.L., 1992. Petrogenetic links among granites and pegmatites in the Harney Peak rare-element granite–pegmatite system, Black Hills, South Dakota. Can. Mineral. 30, 785–809.
Shelley, D., 1993. Igneous and Metamorphic Rocks under the Mcroscope: Classification, Textures, Microstructures and Mineral Preferred Orientations. Chapman & Hall, New York, p. 445.
Shen, X.M., Zhang, H.X., Wang, Q., Wyman, D.A., Yang, Y.H., 2011. Late Devonian-Early Permian A-type granites in the southern Altay Range, Northwest China: petrogenesis and implications for tectonic setting of "A2-type" granites. J. Asian Earth Sci. 42, 986–1007.
Soderlund, U., Patchett, P.J., Vervoort, J.D., Isachsen, C.E., 2004. The ^{176}Lu decay constant determined by Lu–Hf and U–Pb isotope systematics of Precambrian mafic intrusions. Earth Planet. Sci. Lett. 219, 311–324.
Skjerlie, K.P., Johnston, A.D., 1993. Vapor-absent melting at 10 kbar of a biotite- and amphibole-bearing tonalitic gneiss: implications for the generation of A-type granites. Geology 20, 263–266.
Stilling, A., Černý, P., Vanstone, P.J., 2006. The Tanco pegmatite at Bernic Lake, Manitoba. XVI. Zonal and bulk compositions and their petrogenetic significance. Can. Mineral. 44, 599–623.
Su, Y.P., Tang, H.F., Hou, G.S., Liu, C.Q., 2006. Geochemistry of aluminous A-type granites along Dalabut tectonic belt in West Junggar, Xinjiang. Geochimica 35, 55–67.
Sun, M., Yuan, C., Xiao, W., Long, X., Xia, X., Zhao, G., Lin, S., Wu, F., Kröner, A., 2008. Zircon U–Pb and Hf isotopic study of gneissic rocks from the Chinese Altai: progressive accretionary history in the early to middle Palaeozoic. Chem. Geol. 247, 352–383.
Sun, M., Long, X.P., Cai, K.D., Jiang, Y.D., Wong, P.W., Yuan, C., Zhao, G.C., Xiao, W.J., Wu, F.Y., 2009. Early Paleozoic ridge subduction in the Chinese Altai: insight from the abrupt change in zircon Hf isotopic compositions. Sci. China Ser. D 39, 1–14.
Tang, G.J., Wang, Q., Wyman, D.A., Li, Z.X., Zhao, Z.H., Jia, X.H., Jiang, Z.Q., 2010. Ridge subduction and crustal growth in the Central Asian Orogenic Belt: evidence from Late Carboniferous adakites and high-Mg diorites in the western Junggar region, northern Xinjiang (west China). Chem. Geol. 277, 281–300.

Tkachev, A.V., 2011. Evolution and metallogeny of granitic pegmatites associated with orogens throughout geological time. Geol. Soc. London Spec. Publ. 350 (1), 7–23.
Turner, S., Sandiford, M., Foden, J., 1992. Some geodynamic and compositional constraints on 'postorogenic' magmatism. Geology 20, 931–934.
Vervoort, J.D., Pachett, P.J., Gehrels, G.E., Nutman, A.P., 1996. Constraints on early earth differentiation from hafnium and neodymium isotopes. Nature 379, 624–627.
Vervoort, J.D., Patchett, P.J., Blichert-Toft, J., Albarède, F., 1999. Relationships between Lu–Hf and Sm–Nd isotopic systems in the global sedimentary system. Earth Planet. Sci. Lett. 168, 79–99.
Vieira, R., Roda-Robles, E., Pesquera, A., Lima, A., 2011. Chemical variation and significance of micas from the Fregeneda-Almendra pegmatitic field (Central-Iberian Zone Spain and Portugal). Am. Mineral. 96, 637–645.
Vladimirov, A.G., Vystavnoi, S.A., Titov, A.V., Rudnev, S.N., Dergachev, V.B., Annikova, I.Yu., Tikunov, Yu.V., 1998. Petrology of the Early Mesozoic rare-metal granites of the southern Gorny Altai. Geol. Geofiz. (Russian Geology and Geophysics) 39 (7), 901–916 (909–925).
Vladimirov, A.G., Izokh, A.E., Polyakov, G.V., Babin, G.A., Mekhonoshin, A.S., Kruk, N. N., Khlestov, V.V., Khromykh, S.V., Travin, A.V., Yudin, D.S., Shelepaev, R.A., Karmysheva, I.V., Mikheev, E.I., 2013. Gabbro–granite intrusive series and their indicator importance for geodynamic reconstructions. Petrology 21 (2), 158–180.
Wang, D.H., Chen, Y.C., Xu, Z.G., 2002. Metallogenetic Series and Regularity of the Altay Metallogenic Province. Atomic Energy Press, Beijing, pp. 1–493 (in Chinese).
Wang, D.H., Zou, T.R., Xu, Z.G., Yu, J.J., 2004. Advance in the study of using pegmatite deposits as the tracer of orogenic process. Adv. Earth Sci. 19, 614–620 (in Chinese with English abstract).
Wang, D.H., Chen, Y.C., Xu, Z.G., 2003. $^{40}Ar/^{39}Ar$ isotope dating on muscovites from Indosinian rare-metal deposits in Central Altay, Northwestern China. Bull. Mineral. Petrol. Geochem. 22, 14–17 (in Chinese with English abstract).
Wang, X.L., Zhao, G., Zhou, J.-C., Liu, Y., Hu, J., 2008. Geochronology and Hf isotopes of zircon from volcanic rocks of the shuangqiaoshan group, south china: implications for the neoproterozoic tectonic evolution of the eastern jiangnan orogen. Gondwana Res. 14 (3), 355–367.
Wang, Y.J., Yuan, C., Long, X.P., Sun, M., Xiao, W.J., Zhao, G.C., Cai, K.D., Jiang, Y.D., 2011. Geochemistry, zircon U–Pb ages and Hf isotopes of the Paleozoic volcanic rocks in the northwestern Chinese Altai: petrogenesis and tectonic implications. J. Asian Earth Sci. 42, 969–985.
Wang, Y.J., Long, X., Wilde, S., Xu, H., Sun, M., Xiao, W., Yuan, C., Cai, K., 2014. Provenance of Early Paleozoic metasediments in the central Chinese Altai: implications for tectonic affinity of the Altai-Mongolia terrane in the Central Asian Orogenic Belt. Lithos 210–211, 57–68.
Wang, T., Hong, D.W., Jahn, B.M., Tong, Y., Wang, Y.B., Han, B.F., Wang, X.X., 2006. Timing, petrogenesis, and setting of Paleozoic synorogenic intrusions from the Altai Mountains, Northwest China: implications for the tectonic evolution of an accretionary orogen. J. Geol. 114, 735–751.
Wang, T., Tong, Y., Jahn, B.M., Zou, T.R., Wang, Y.B., Hong, D.W., Han, B.F., 2007. SHRIMP U–Pb Zircon geochronology of the Altai No. 3 Pegmatite, NW China, and its implications for the origin and tectonic setting of the pegmatite. Ore Geol. Rev. 32, 325–336.
Webster, J.D., Thomas, R., Rhede, D., Forster, H.J., Seltmann, R., 1997. Melt inclusions in quartz from an evolved peraluminous pegmatite: geochemical evidence for strong tin enrichment in fluorine-rich and phosphorus-rich residual liquids. Geochim. Cosmochim. Acta 61, 2589–2604.
Wedepohl, K.H., 1995. The composition of the continental crust. Geochim. Cosmochim. Acta 59, 1217–1232.
Windley, B.F., Kröner, A., Guo, J., Qu, G., Li, Y., Zhang, C., 2002. Neoproterozoic to Palaeozoic geology of the Altai orogen, NW China: new zircon age data and tectonic evolution. J. Geol. 110, 719–739.
Windley, B.F., Alexeiev, D., Xiao, W., Kroner, A., Badarch, G., 2007. Tectonic models for accretion of the Central Asian Orogenic Belt. J. Geol. Soc. London 164, 31–47.
Woodhead, J., Hergt, J., Shelley, M., Eggins, S., Kemp, R., 2004. Zircon Hf-isotope analysis with an excimer laser, depth profiling, ablation of complex geometries, and concomitant age estimation. Chem. Geol. 209, 121–135.
Wu, B.Q., Zou, T.R., 1989. The genesis of granitic pegmatites in Xinjiang Altai. Min. Geol. Xinjiang 1, 60–70 (in Chinese).
Wu, F.Y., Yang, Y.H., Xie, L.W., Yang, J.H., Xu, P., 2006. Hf isotopic compositions of the standard zircons and baddeleyites used in U–Pb geochronology. Chem. Geol. 234, 105–126.
Wyllie, P.J., Sekine, T., 1982. The formation of mantle phlogopite in subduction zone hybridization. Contrib. Miner. Petrol. 79, 375–380.
Xiao, W.J., Windley, B.F., Badararch, G., Li, J., Sun, S., Qin, K., Wang, Z., 2004. Palaeozoic accretionary and convergent tectonics of the southern Altaids: implications for the growth of central Asia. J. Geol. Soc. London 161, 1–4.
Xiao, W.J., Han, C.M., Yuan, C., Sun, M., Lin, S.F., Chen, H.L., Li, Z.L., Li, J.L., Sun, S., 2008. Middle Cambrian to Permian subduction-related accretionary orogenesis of Northern Xinjiang, NW China: implications for the tectonic evolution of central Asia. J. Asian Earth Sci. 32, 102–117.
Xiao, W.J., Kröner, A., Windley, B.F., 2009. Geodynamic evolution of Central Asia in the Paleozoic and Mesozoic. Int. J. Earth Sci. 98, 1185–1188.
Xiao, W.J., Huang, B.C., Han, C.M., Sun, S., Li, J.L., 2010. A review of the western part of the Altaids: a key to understanding the architecture of accretionary orogens. Gondwana Res. 18, 253–273.
Xiao, W.J., Santosh, M., 2014. The western Central Asian Orogenic Belt: a window to accretionary orogenesis and continental growth. Gondwana Res. 25 (4), 1429–1444.
Xu, P., Wu, F.Y., Xie, L.W., Yang, Y.H., 2004. Hf isotopic compositions of the standard zircons for U–Pb dating. Chin. Sci. Bull. 49, 1642–1648.
Yakubchuk, A.S., 2004. Architecture and mineral deposit settings of Altaid orogenic collage: a revised model. J. Asian Earth Sci. 23, 761–779.
Yin, R., Wang, R., Zhang, A., Hu, H., Zhu, J., Rao, C., Zhang, H., 2013. Extreme fractionation from zircon to hafnon in the Koktokay No. 1 granitic pegmatite, Altai, northwestern China. Am. Mineral. 98, 1–6.
Yuan, C., Sun, M., Xiao, W.J., Li, X.H., Chen, H.L., Lin, S.F., Xia, X.P., Long, X.P., 2007. Accretionary orogenesis of the Chinese Altai: insights from Paleozoic granitoids. Chem. Geol. 242, 22–39.
Zagorsky, V.Ye., Shokalsky, S.P., Sergeev, S.A., 2015. Age, duration of formation, and geotectonic position of the zavitaya lithium granite–pegmatite system, Eastern Transbaikalia. Doklady Earth Sci. 460 (1), 16–21.
Zhang, X., Zhang, H., 2014. Geochronological, geochemical, and Sr–Nd–Hf isotopic studies of the Baiyanghe A-type granite porphyry in the Western Junggar: implications for its petrogenesis and tectonic setting. Gondwana Res. 25, 1554–1569.
Zhao, Z.F., Zheng, Y.F., Wei, C.S., Wu, Y.B., 2007. Post-collisional granitoids from the Dabie orogen in China: zircon U–Pb age, element and O isotope evidence for recycling of subducted continental crust. Lithos 93, 248–272.
Zhou, T.F., Yuan, F., Fan, Y., Zhang, D.Y., Cooke, D., Zhao, G.C., 2008. Granites in the Sawuer region of the west Junggar, Xinjiang Province, China: geochronological and geochemical characteristics and their geodynamic significance. Lithos 106, 191–206.
Zhu, Y.F., Zeng, Y., Gu, L., 2006. Geochemistry of the rare metal-bearing pegmatite No. 3 vein and related granites in the Keketuohai region, Altay Mountains, northwest China. J. Asian Earth Sci. 27 (1), 61–77.